



Variations in eastern Mediterranean hydrology during the last climatic cycle as inferred from neodymium isotopes in foraminifera

Maxence Duhamel^a, Christophe Colin^{a,*}, Marie Revel^b, Giuseppe Siani^a,
Arnaud Dapoigny^c, Eric Douville^c, Jiawang Wu^d, Yulong Zhao^d, Zhifei Liu^d,
Paolo Montagna^e

^a Université Paris-Saclay, CNRS, GEOPS, Orsay, 91405, France

^b Université de la Côte d'Azur, CNRS, OCA, IRD, Geoazur, 250 rue Albert Einstein, 06500, Valbonne, France

^c Laboratoire des Sciences du Climat et de l'Environnement, LSCE/IPSL, CEA-CNRS-UVSQ, Université Paris-Saclay, F-91191, Gif-sur-Yvette, France

^d State Key Laboratory of Marine Geology, Tongji University, Shanghai, 200092, China

^e ISP-CNR, Via Gobetti 101, 40129, Bologna, Italy

ARTICLE INFO

Article history:

Received 22 December 2019

Received in revised form

3 April 2020

Accepted 3 April 2020

Available online xxx

Keywords:

Neodymium isotopes

Foraminifera

Paleo-hydrology

Sapropels

Eastern Mediterranean sea

African monsoon

ABSTRACT

The Nd isotopic compositions (ϵNd) of mixed planktonic foraminifera have been analyzed in two sediment cores collected in the Nile deep-sea fan in order to reconstruct past ϵNd of the Eastern Mediterranean Deep Water (EMDW) and to assess the relative contributions of Nile discharge and Modified Atlantic Water (MAW) inflow to the Eastern Mediterranean Sea hydrology, as well as their potential control on anoxic events over the last climatic cycle. The two foraminiferal ϵNd records are similar and display an increase in ϵNd values during the African Humid Periods. Superimposed on this precession-forced variability (insolation received by the Earth at low latitudes), the record of variations in foraminiferal ϵNd indicates a 2-unit decrease in ϵNd during the interglacial Marine Isotope Stages (MIS) 5 and 1 compared to glacial MIS6, 4, 3 and 2. The ϵNd results suggest that the long-term glacial to interglacial changes in Nd isotopic composition of EMDW were not entirely induced by variations in Nile River discharge and Saharan dust inputs. Decreases in ϵNd during MIS5 and MIS1 interglacials indicate an increase in the contribution of unradiogenic MAW to the eastern Mediterranean Sea related to high sea-level stands and greater seawater exchange between the North Atlantic and Mediterranean basins. In addition, radiogenic seawater ϵNd values observed during African Humid Periods (and sapropel events) are associated with an intensification of Nile discharge and an increase in residence time of deep-water masses in the eastern Mediterranean Sea, which induces an increase in the interaction between deep-water masses and radiogenic sediments along the margin of the eastern Mediterranean Sea. Results confirm that an intensification of the hydrological exchanges between the western and eastern Mediterranean basins during high sea-level stand and the subsequent higher proportion of Atlantic Water in the Levantine Basin may have preconditioned the eastern Mediterranean Sea to sapropel depositions during the last climatic cycle.

© 2020 Elsevier Ltd. All rights reserved.

1. Introduction

The Mediterranean Sea is a semi-enclosed basin, where an excess of evaporation over precipitation and runoff induces a characteristic eastward increase in the salinity of the surface Atlantic water that enters through the Gibraltar Strait and flows to

the eastern Mediterranean basin; this water effectively becomes denser and contributes to the formation of intermediate and deep waters. The resulting Mediterranean thermohaline circulation has been demonstrated to be highly sensitive to present-day and past climate changes in both high and low latitudes (Rossignol-Strick et al., 1982; Roether et al., 1996; Kallel et al., 1997; Pinardi and Masetti, 2000; Rohling et al., 2002; Emeis et al., 2003; Scrivner et al., 2004; Melki et al., 2009; Revel et al., 2010; Toucanne et al., 2015; Filippidi et al., 2016; Tesi et al., 2017). This variability is thought to be responsible for the deposition of organic-rich

* Corresponding author.

E-mail address: christophe.colin@universite-paris-saclay.fr (C. Colin).

sapropel layers (characterized by $>1\%$ C_{org}) in the Eastern Mediterranean Sea (EMS) (Murat et al., 2000) and of Organic Rich Levels (ORL) in the Western Mediterranean Sea (WMS) (e.g. Rohling et al., 2015). However, paleo-hydrological processes and associated ventilation dynamics related to sapropel deposition are still debated because conventional water-mass proxies, such as $\delta^{13}C$ analyzed on benthic foraminifera, cannot be used systematically due to the lack of benthic foraminifera in EMS sediments during time intervals when bottom waters were characterized by anoxic conditions.

Despite many unresolved problems, such as the processes responsible for the sluggish thermohaline circulation during deep-sea anoxic events, significant advances have been made over recent decades in our understanding of sapropel formation since the pioneering work of Rossignol-Strick et al. (1982). There is now a common consensus that the formation of sapropels in the Mediterranean Sea is closely linked to: (1) reduced deep-water ventilation associated to freshwater input lowering surface water salinity, thus causing stratification of the water masses with limited or no oxygen renewal in deep water; or (2) nutrient-rich surface freshwater inputs, which significantly increase surface productivity and induce the mineralization of organic matter in deep water to a level that exceeds oxygen inputs through deep water mass renewal; or (3) a combination of both processes (Rohling, 1994; Cramp and O'Sullivan, 1999; Rohling et al., 2015). The leading role of stratification in most studied sapropels is revealed by the neodymium (Nd) isotopic composition of biogenic/ authigenic fractions (e.g. Freydisier et al., 2001; Cornuault et al., 2018; Wu et al., 2019), benthic foraminifera carbon isotopic records, faunal assemblages (e.g. Schmiedl et al., 2010; Cornuault et al., 2016), redox-sensitive elemental compositions (e.g. Jilbert et al., 2010; Tachikawa et al., 2015; Tesi et al., 2017), and circulation models (e.g. Myers et al., 1998a, b; Myers, 2002; Stratford et al., 2000; Bianchi et al., 2006; Grimm et al., 2015; Vadsaria et al., 2019).

Many studies have confirmed that periods of sapropel deposition are marked by high river runoff originating from the low-latitude monsoonal system, whereas time intervals between sapropel depositions are arid with reduced riverine runoff and increased wind-blown sediment supplies (e.g. Wehausen and Brumsack, 1999; Larrasoana et al., 2003; Zhao et al., 2012; Revel et al., 2014). A widely accepted explanation for the excess freshwater input during times of sapropel formation is related to heavy monsoonal precipitation in North Africa which was channeled by the Nile River and other North African paleo-rivers (e.g. Rossignol-Strick et al., 1982; Fontugne et al., 1994; Rohling et al., 2002; Emeis et al., 2003; Scrivner et al., 2004; Osborne et al., 2008, 2010; Revel et al., 2010; Wu et al., 2016, 2017). In North Africa, these humid periods have been attributed to the northward migration of the rain belt associated with the Inter-Tropical Convergence Zone (ITCZ) due to precession-driven insolation changes (Rossignol-Strick et al., 1982; DeMenocal et al., 2000; Gasse, 2000; Arbuszewski et al., 2013; Skonieczny et al., 2015, 2019). The last period of more intense rainfall compared to the present, the so-called African Humid Period (AHP: from ~14.8 to ~6 cal kyr BP; Shanahan et al., 2015; Bastian et al., 2017), is thought to be responsible for the formation of the organic-rich sapropel S1 in the EMS between 10.2 and 6.4 cal kyr BP (Mercone et al., 2000; De Lange et al., 2008). Thus, the strong correspondence between sapropel formation and periods of African monsoon intensification, when freshwater discharge by North African rivers into the Mediterranean Sea increased, suggests that the reduction in sea surface salinity and deep-water convection could be the result of changes in the African monsoon system (Revel et al., 2015; Rohling et al., 2015). However, enhanced freshwater inputs from the northern margin of the Mediterranean Sea related to precipitations driven by westerly

winds and the melting of glacial ice-sheets and linked to climate changes in the high latitudes of the Northern hemisphere (e.g. Kallel et al., 1997; Emeis et al., 2003; Melki et al., 2009; Toucanne et al., 2015; Filippidi et al., 2016; Tesi et al., 2017) would have also led to the reduction of deep-water formation in the EMS, limiting the oxygen supply to the deep water (Rohling, 1994). Furthermore, several studies have shown that the Mediterranean thermohaline circulation is sensitive to rapid climatic changes in the northern hemisphere (e.g. Heinrich and Dansgaard - Oeschger events) (Rohling et al., 1995; Kallel et al., 1997; Allen et al., 1999; Bartov et al., 2003; Martrat et al., 2004).

In addition, the narrow and shallow Siculo-Tunisian and Gibraltar Straits tend to limit exchanges between the eastern and western Mediterranean basins, and with the North Atlantic. It has been proposed that water exchanges through the Straits may have been significantly limited during the glacial low sea-level stands of the late Quaternary. A general circulation model has shown that Mediterranean water outflow was reduced by 50% during the Last Glacial Maximum (LGM) (Mikolajewicz, 2011), and several studies have pointed to a salinity increase in the eastern basin (Thunell and Williams, 1989; Myers et al., 1998a). In particular, Mikolajewicz (2011) has shown that the formation of deep waters in the eastern basin during the LGM was strengthened and that these waters were principally formed in the Aegean Sea and not in the Adriatic Sea as is the case today. It has also been proposed that rising global sea level during deglaciation led to greater exchanges between the basins and a drop in surface salinity, thus preconditioning the sapropel event by slowing down intermediate and deep convections (Grimm et al., 2015).

Studies of past changes in Mediterranean thermohaline circulation have mostly investigated the last glacial period, focusing on the deposition of sapropel S1 (10.2–6.4 cal kyr BP; Mercone et al., 2000) (e.g. Cacho et al., 2002; Sierro et al., 2005; Frigola et al., 2008; Schmiedl et al., 2010; Toucanne et al., 2012; Angue Minto'o et al., 2015; Jiménez-Espejo et al., 2015). Continuous $\delta^{13}C$ and $\delta^{18}O$ records from epibenthic foraminifera of the last glacial – interglacial climatic cycle are rare and difficult to obtain for bottom suboxic or anoxic environments (e.g. sapropel events) in the EMS. This is due to the lack of a continuous population of epibenthic foraminifera species for which a calibrated vital effect for $\delta^{13}C$ analyses is well established (Schmiedl et al., 2003, 2010). Consequently, the hydrological pattern of the EMS is not well constrained for periods of sapropel deposition and for the time intervals that preconditioned such events.

In the present study, we have investigated the Nd isotopic composition (ϵNd) of the diagenetic Fe–Mn coatings precipitated on foraminifera shells. It has been demonstrated that ϵNd measured on planktonic foraminifera shells represents mainly bottom seawater and/or pore water ϵNd (Tachikawa et al., 2013, 2014). Such ϵNd obtained from foraminiferal shells have been previously used to provide information on water mass provenance and mixing in the ocean (Molina-Kescher et al., 2014; Wu et al., 2015b, 2019; Dubois-Dauphin et al., 2017; Cornuault et al., 2018). Modern Mediterranean seawater displays a wide range of ϵNd values, from –11 to –5, with unradiogenic surface water entering the Mediterranean as Atlantic Water and more radiogenic intermediate and deep waters originating from the Levantine Basin (Henry et al., 1994; Tachikawa et al., 2004; Vance et al., 2004). With a residence time of 500–1000 years (Tachikawa et al., 2003; Siddall et al., 2008) and distinct local basin-scale sources, ϵNd is assumed to behave quasi-conservatively, with great potential to fingerprint the provenance of Mediterranean water masses (Dubois-Dauphin et al., 2017; Cornuault et al., 2018; Wu et al., 2019).

The ϵNd of mixed planktonic foraminifera from two sediment cores collected in the Levantine Basin were investigated in order to

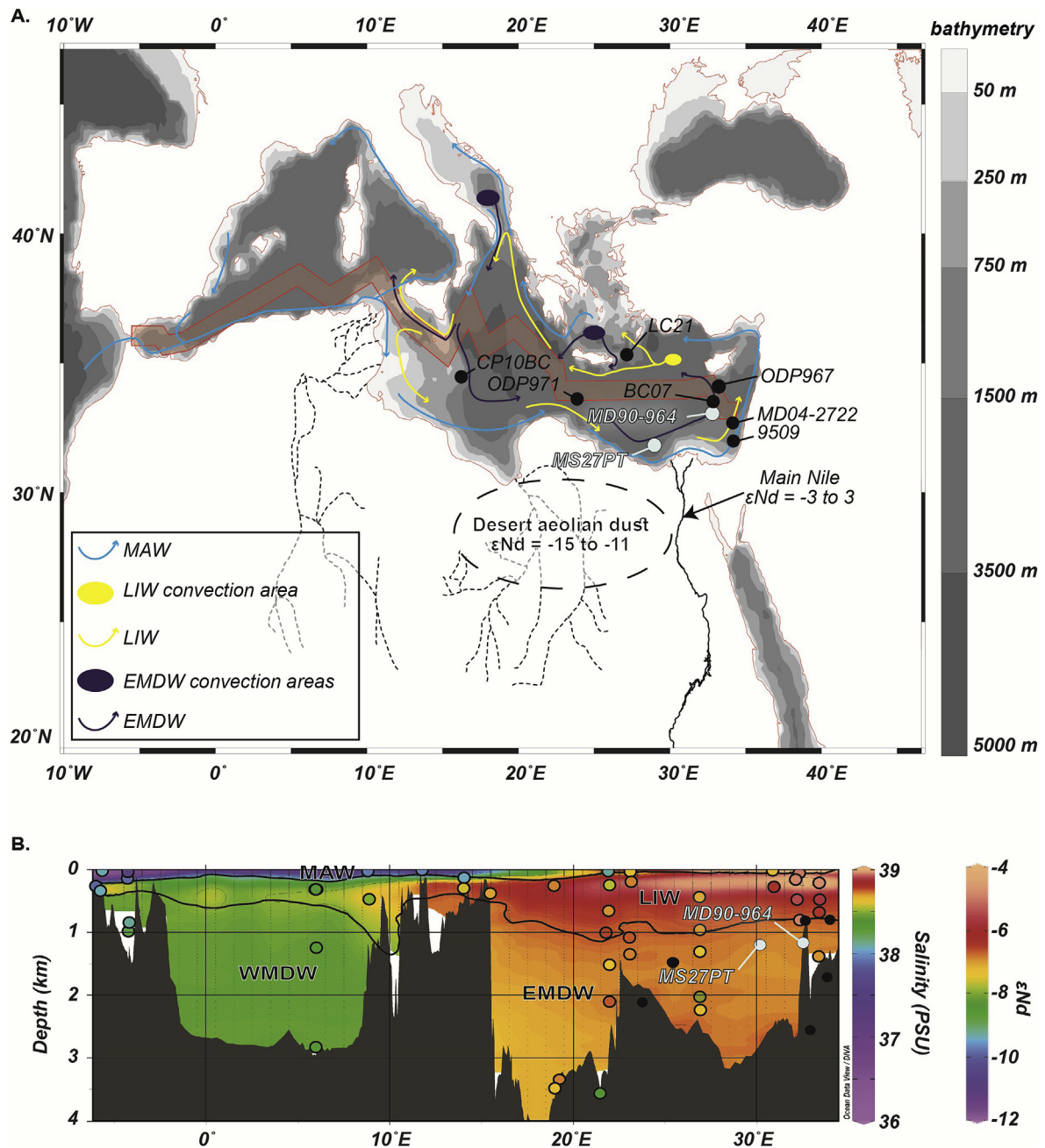


Fig. 1. (A) Bathymetric map of the Mediterranean Sea showing locations of core MD90-964 ($33^{\circ}02.75'N$; $32^{\circ}38.57'E$; water depth 1375 m, length 32.12 m), core MS27PT ($31^{\circ}47.90'N$, $29^{\circ}27.70'E$; water depth 1389 m, length 7.3 m) (blue dots) and all the other sites discussed in this study (black dots) (Freydier et al., 2001; Scrivner et al., 2004; Osborne et al., 2008, 2010; Cornuault et al., 2018). The simplified modern Mediterranean water circulation is broadly indicated. Signatures of Nd isotopic composition are displayed for the Nile River and aeolian dust (Padoan et al., 2011; Scheuven et al., 2013). The potential pathways of North-African paleo-rivers are also depicted in light gray (Rohling et al., 2002; Wu et al., 2017). (B) Longitudinal transect of annual mean salinity of the Mediterranean Sea (i.e. the red shading shown in (A); data from WOA13). ϵNd values are represented by colored dots (Henry et al., 1994; Tachikawa et al., 2004; Vance et al., 2004). The map and section were generated using Ocean Data View software. (For interpretation of the references to color in this figure legend, the reader is referred to the Web version of this article.)

reconstruct past ϵNd of the EMDW over the last 145 kyr. Combined with previous ϵNd records, the new results allow us to assess the relative contributions of Nile discharge and inflow of Modified Atlantic Water (MAW) to the thermohaline circulation of the EMS over the last climatic cycle characterized by several anoxic events and the deposition of sapropels S1 to S5. This allows us to constrain the hydrology at the origin of these anoxic events under different environmental conditions (different sea levels, different freshwater supplies from the African rivers and different hydrological exchange conditions at the Gibraltar and the Siculo-Tunisian Straits).

2. Regional hydrological setting in terms of ϵNd

The Mediterranean Sea is an almost enclosed basin that exchanges surface and intermediate waters with the Atlantic Ocean through the Gibraltar Strait (sill depth ~ 300 m) and surface water with the Black Sea through the Dardanelles Strait (sill depth ~ 100 m). Driven by a negative water budget, an anti-estuarine circulation occurs in the Mediterranean Sea. Hence, the relatively fresh surface Atlantic Water (AW) (salinity ~ 36.5), which has an unradiogenic ϵNd signature of ~ -9.7 (Tachikawa et al., 2004), flows

into the WMS and is then modified by mixing with the ambient surface water to reach ~ -10.4 in the Alboran Sea (Tachikawa et al., 2004; Spivack and Wasserburg, 1988). During its eastward flow, AW mixes with the surrounding surface waters and underlying intermediate waters leading to the formation of the Modified Atlantic Water (MAW) that flows along the basin at 50–200 m water depth following a general cyclonic flow path with several eddies and meanders (Fig. 1). The ϵNd values for MAW range from -10.8 to -9.0 in the western basin (Henry et al., 1994) and from -9.8 to -4.9 in the eastern basin (Tachikawa et al., 2004; Vance et al., 2004). Since evaporation exceeds precipitation and river runoff, the relatively fresh surface AW flowing into the WMS also becomes progressively saltier (~ 38.5) as it circulates eastward.

During winter time, intense cooling and strong wind-induced heat loss produce denser waters that sink via convection and form the intermediate waters in the Aegean Sea and the Levantine Basin and deep waters in the Gulf of Lions and the Adriatic Sea (Robinson et al., 2001; Schroeder et al., 2012). In particular, the Levantine Intermediate Water (LIW) is formed in the Cyprus-Rhodes area and it spreads westwards throughout the entire Mediterranean Basin at depths of between ~ 150 and 700 m (Lascaratos et al., 1993; Malanotte-Rizzoli et al., 1999). The LIW acquires its ϵNd signature mainly from the partial dissolution of particles from the Nile River and the Egyptian/Libyan margin sediments of the EMS, which have ϵNd values ranging from -7 to -2 (Weldeab et al., 2002a; Tachikawa et al., 2004; Ayache et al., 2016). This more radiogenic Nd signature is explained by sediment originating from the erosion of Ethiopian traps including Cenozoic basaltic silicate rocks ($\epsilon\text{Nd} > 0$) (Garzanti et al., 2015). The LIW is thus characterized by a radiogenic ϵNd of ~ -4.8 in the eastern part of the EMS and by an east-west ϵNd gradient ranging from -4.8 to -9.2 , resulting from mixing with overlying and underlying water masses along its path (Henry et al., 1994; Tachikawa et al., 2004; Vance et al., 2004). In the Adriatic Sea, LIW is involved in the formation of Adriatic Deep Water (AdDW) that sinks into the deep EMS contributing, together with the Aegean Deep Water (AeDW), to the formation of the Eastern Mediterranean Deep Water (EMDW). The EMDW ϵNd values range from -7 to -6 with an average value of -6.5 (Tachikawa et al., 2004). The Western Mediterranean Deep Water (WMDW) is formed in the Gulf of Lions in winter, as a result of mixing between the relatively fresh surface water and the saline LIW; it then spreads into the Balearic Basin and Tyrrhenian Sea between ~ 2000 and ~ 3000 m (Millot, 1999; Schroeder et al., 2012) (Fig. 1). The WMDW is characterized by an average ϵNd value of -9.4 ± 0.9 (Henry et al., 1994; Tachikawa et al., 2004). Between the WDMW and the LIW (from ~ 700 to ~ 2000 m), the Tyrrhenian Deep Water (TDW) (Millot et al., 2006), which is produced by mixing between WMDW and EMDW, has an average ϵNd value of -8.1 ± 0.5 .

The Blue Nile and Atbara rivers represent together 97% of the suspended sediment load and 68% of the freshwater supply of the total annual Nile discharge (Foucault and Stanley, 1989; Williams et al., 2000; Revel et al., 2015). ϵNd signatures of sediments from the Nile Basin are characterized by contrasted signatures, ranging from radiogenic values ($\epsilon\text{Nd} \approx 0$) for the Cenozoic Ethiopian traps to strongly unradiogenic values ($\epsilon\text{Nd} \approx -30$) for the Precambrian Central Africa Craton (Garzanti et al., 2015). Sediments from the Bahr el Jebel (between Lake Albert and 10°N of latitude) are characterized by a ϵNd value of -25 , whereas Victoria-Albert Nile-derived fluvial muds by a range from -29 to -36 (Padoan et al., 2011). The Equatorial-White Nile sediment makes up approximately 3.5% of the present-day total sediment discharge of the Nile and is fairly constant throughout the year (Blanchet et al., 2015; Garzanti et al., 2015), with a very unradiogenic signature (from -30 to -35). In contrast, the Blue Nile sediment, which is mainly

transported during the humid phase, dominates the total sediment discharge of the Nile (72%) and is characterized by very radiogenic ϵNd values (from -3 to 5 ; Padoan et al., 2011; Blanchet et al., 2013; Garzanti et al., 2015).

3. Material and methods

3.1. Studied cores

For this study, we have selected cores MD90-964 and MS27PT, which are bathed by the Eastern Mediterranean Deep Water (EMDW).

Core MD90-964 ($33^\circ 02.75'\text{N}$, $32^\circ 38.57'\text{E}$; water depth 1375 m, length 32.12 m) was collected on the eastern part of the Nile deep-sea fan during the PROMETE III campaign on board R/V Marion Dufresne in September 1990 (Fig. 1). Core MD90-964 sediments consist of pale cream to yellowish brown foraminiferal and nanofossil marl ooze, interbedded with sapropelic layers that vary in thickness from 2 to 41 cm (Zhao et al., 2011). The $\delta^{18}\text{O}$ of *Globigerinoides ruber*, clay mineralogy, total organic carbon (TOC) content and elemental intensities by X-ray fluorescence (XRF) have been studied previously by Zhao et al. (2011). The age model of core MD90-964 (Zhao et al., 2011) has been established by correlating the *G. ruber* $\delta^{18}\text{O}$ record and the Mediterranean *G. ruber* stack compiled by Lourens (2004), using Gaussian filtering at both obliquity and precession, and cross-spectral analysis against a target curve that reflects characteristics of orbital parameters (ETP curve). According to the age model, the upper 7.30 m of core MD90-964 investigated in this study cover the last 145 kyr and present a linear mean sedimentation rate of 5 cm/kyr. Sapropels S1, S3, S4 and S5 are identified by an increase of C_{org} content, which reaches up to 6% during the deposition of sapropel S5 (Fig. 2; Zhao et al., 2011).

Core MS27PT ($31^\circ 47.90'\text{N}$, $29^\circ 27.70'\text{E}$; water depth 1389 m, length 7.3 m) was retrieved on the western Nile delta, around 90 km from the mouth of the Rosetta Nile River, during the Mediflux MIMES cruise of the R/V Pelagia in 2004 (Fig. 1). The core site lies directly under the influence of the Nile freshwater discharge. For this study, we have investigated the upper 3.15 m of core MS27PT which consist of carbonate-rich facies with coarse quartz grains and clastic mud-rich facies where sapropel S1 has been identified (Revel et al., 2010) (Fig. 2). The age model of the studied interval of core MS27PT is based on 22 previously published AMS ^{14}C dates (Revel et al., 2010, 2015; Bastian et al., 2017; Ménot et al., 2020) (Fig. 2).

4. Methods

The samples investigated in this study consist of 15–30 mg of mono-specific planktonic foraminifera *G. ruber* and mixed planktonic foraminifera, hand-picked in the $>150 \mu\text{m}$ size fraction. Cleaning procedure and purification of Nd have been done in a class 100 clean laboratory using ultrapure reagents. All of the test samples were crushed between two glass slides to open the foraminiferal chambers. The calcite fragments were then ultrasonicated for 1 min before pipetting off the suspended particles with water to separate the waste. This step was repeated until the water became clear and free of clay. All samples were checked under a binocular microscope to ensure that all particles had been removed. Most of the samples were then analyzed after this preliminary physical cleaning step (hereafter referred as “uncleaned foraminifera”) (Wu et al., 2015b).

For this study, some physically cleaned samples were transferred to centrifuge tubes for an oxidative-reductive cleaning step (hereafter referred as “cleaned foraminifera”). The oxidative-

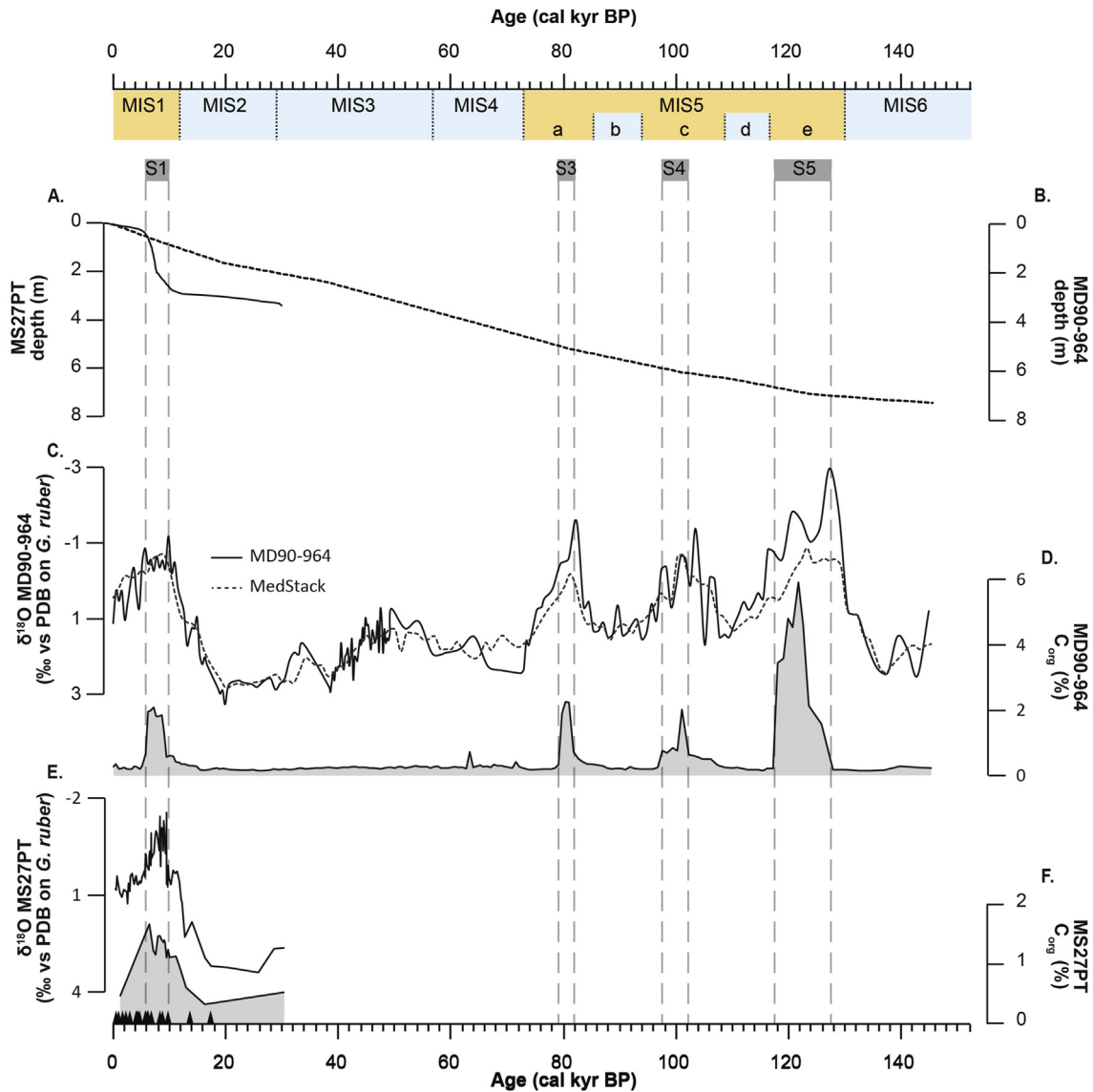


Fig. 2. Age models of cores MD90-964 and MS27PT: (A) age-depth curve for core MS27PT (continuous line) interpolated from AMS ^{14}C dates (Revel et al., 2015; Bastian et al., 2017) and (B) age-depth curve for core MD90-964 (dashed line) (Zhao et al., 2011). (C) $\delta^{18}\text{O}$ analyzed on planktonic foraminifera *G. ruber* of core MD90-964 (continuous line) and MedStack composite reference (dashed line; Lourens, 2004). (D) Organic carbon concentration of core MD90-964 sediment (Zhao et al., 2011). (E) $\delta^{18}\text{O}$ analyzed on *G. ruber* of core MS27PT. (F) Organic carbon concentration of core MS27PT sediment. Black triangles correspond to the radiocarbon dates obtained for core MS27PT. The Marine Isotope Stages (MIS) and time intervals of sapropel layers are also reported.

reductive foraminiferal cleaning procedure followed that described by Vance and Burton (1999), using 10 ml reductive solution (1 M hydrazine, 16 M NH_4OH , 0.25 M citric acid in a ratio of 1:6:3) and 5 ml oxidative solution (0.2 M NaOH and 30% H_2O_2 in a 1:1 ratio) per sample to more efficiently remove authigenic Fe–Mn coatings and organic material. For the reductive step, samples were heated in a water bath at 80 °C for 30 min, and were ultrasonicated every 3 min for 10 s. After transferring the reductive cleaning solution to a centrifuge tube, the cleaned foraminifera were rinsed with Milli-Q water. The analytical procedure for the oxidative step was similar except that samples were ultrasonicated every 10 min for a period of 30 s.

All samples, including uncleaned foraminifera, underwent weak acid leaching for 5 min in 1 ml 0.001 M HNO_3 with ultrasonication. After these cleaning steps, samples were transferred into a 1.5 ml tube. 0.5 ml of Milli-Q water was first added to the tube, and then the foraminifera were dissolved using stepwise 100 μl 0.5 M HNO_3

until the dissolution reaction stopped. The dissolved samples were centrifuged, and the supernatant was immediately transferred to Teflon beakers to prevent leaching of any possible remaining phases. The dissolved foraminifera shell fractions and authigenic fractions contained in the reductive cleaning solution were dried using a hotplate for Nd extraction. Nd was purified using Eichrom TRU-Spec and Ln-Spec resins following the detailed analytical procedures described in Copard et al. (2010). The $^{143}\text{Nd}/^{144}\text{Nd}$ ratios were measured using the ThermoScientific Neptune^{plus} Multi-Collector Inductively Coupled Plasma Mass Spectrometer (MC-ICP-MS), hosted at the Laboratoire des Sciences du Climat et de l'Environnement (LSCE) in Gif-sur-Yvette. For the Nd isotope analyses, sample and standard concentrations were matched at 10 ppb. Mass-dependent fractionation was corrected by normalizing $^{146}\text{Nd}/^{144}\text{Nd}$ to 0.7219 and applying an exponential law. During the analytical sessions, every set of two samples was bracketed by analyses of the La Jolla Nd standard solution, which is characterized

by certified values of 0.511858 ± 0.000007 (Lugmair et al., 1983). The offset value between results and certified values of La Jolla standard was lower than 0.4 epsilon units (ϵNd) for all of the analyses presented in this study. The analytical errors reported herein correspond to the external 2 sigma standard deviation (based on repeated analyses of the La Jolla standard for the different analytical sessions) and range from 0.1 to 0.5 ϵNd (Table 1 and Table 2). The analytical blank values for Nd evaluated by using a quadrupole ICPMS were <4 pg, which represents less than 0.1% of the minimum Nd yield from foraminifera used in this study. As a result, no blank correction was applied. Results are expressed as $\epsilon\text{Nd} = [(^{143}\text{Nd}/^{144}\text{Nd})_{\text{sample}} / (^{143}\text{Nd}/^{144}\text{Nd})_{\text{CHUR}} - 1] * 10,000$, with the present-day $(^{143}\text{Nd}/^{144}\text{Nd})_{\text{CHUR}}$ of 0.512638 (Jacobsen and Wasserburg, 1980).

5. Results

5.1. The ϵNd record of cores MS27PT and MD90-964

The ϵNd values from core MS27PT, obtained on both monospecific samples of planktonic foraminifer *G. ruber* and mixed planktonic foraminifera, exhibit a wide range from -5.71 ± 0.13 to -2.51 ± 0.21 (Table 1 and Fig. 3). The ϵNd values of monospecific and mixed samples from the same sediment volume are in agreement within an uncertainty of 2 sigma (Table 1). It is worth noting that mean ϵNd values obtained from foraminifera cleaning solutions are similar or slightly more radiogenic than cleaned foraminifera. This confirms that oxidative-reductive cleaning procedures applied to foraminiferal tests from our sampling sites are not effective to fully remove the Nd associated with the authigenic

Fe–Mn coating (Wu et al., 2015b). Therefore, ϵNd obtained in both reductively cleaned and non-reductively cleaned foraminifera are associated with bottom and/or pore-water ϵNd values as it has been demonstrated elsewhere for a large compilation of ϵNd results obtained from foraminifera (Tachikawa et al., 2014).

For core MS27PT, ϵNd displays lower values of -4.7 ± 0.2 to -4.9 ± 0.1 between 21 and 16.4 cal kyr BP (Fig. 3). It increases to more radiogenic values (-2.5 ± 0.2 to -4.4 ± 0.3) in the time interval between 14.1 and 6.8 cal kyr BP, corresponding to the AHP which is associated with higher Nile flood discharges (DeMenocal et al., 2000; Revel et al., 2015; Castañeda et al., 2016). The highest value (-2.5 ± 0.2) is recorded at 9.7 cal kyr BP. The ϵNd values then steadily decrease from -2.5 ± 0.2 to -5.5 ± 0.3 between 9.7 and 4.3 cal kyr BP. The time interval coeval with the period during which sapropel S1 was deposited (10.2–6.4 cal kyr BP) is associated with radiogenic ϵNd values (from -2.7 ± 0.2 to -4.3 ± 0.2). The time interval between 4.3 and 1.5 cal kyr BP presents unradiogenic ϵNd values (up to -5.9 ± 0.1) which increase again thereafter to reach -4.0 ± 0.1 at the core top.

For core MD90-964, ϵNd values were obtained for samples of uncleaned mixed foraminifera from the Marine Isotope Stage (MIS) 6 to the Holocene (Fig. 4E). In general, glacial MIS6, MIS4, MIS3 and MIS2 are characterized by high ϵNd values, ranging from -3.8 ± 0.2 to -2.8 ± 0.2 . In contrast, interglacial MIS5 and the Late Holocene display lower ϵNd values, from -4.5 ± 0.2 to -2.8 ± 0.3 . Superimposed on this long-term glacial-interglacial variation, the monsoon–precession induced signal is distinguished by more radiogenic values related to the African Humid Periods (from 123.5 to 121.7 cal kyr BP, 102.3 to 99.3 cal kyr BP, 84.3 to 81.8 cal kyr BP; 55 cal kyr BP and 9.5 to 6.2 cal kyr BP) (e.g. Gasse, 2000; Zhao et al.,

Table 1
Results of Nd isotopic composition obtained from planktonic foraminifera samples from core MS27PT. Nd isotopic composition were obtained from reductively cleaned foraminifera, cleaning solution, or uncleaned foraminifera. Foraminifera are monospecific (*G. ruber*) or multispecific (mixed planktonic foraminifera). The age of sediments have been determined by linear interpolation between 22 AMS¹⁴C dates of foraminifera (Revel et al., 2010, 2015; Bastian et al., 2017; Menot et al., 2020).

Depth (cm)	Age (cal kyr BP)	¹⁴³ Nd/ ¹⁴⁴ Nd	±2σ	εNd	±2σ	Samples
0.5	0.7	0.512432	±0.000008	-4.03	±0.17	uncleaned mixed planktonic foraminifera
2.5	1.3	0.512399	±0.000008	-4.67	±0.16	uncleaned mixed planktonic foraminifera
6	2.4	0.512345	±0.000007	-5.71	±0.13	cleaned mixed planktonic foraminifera
6	2.4	0.512351	±0.000007	-5.61	±0.13	cleaned <i>G. ruber</i>
6	2.4	0.512332	±0.000018	-5.97	±0.35	cleaning solution, mixed planktonic foraminifera
6	2.4	0.512335	±0.000008	-5.91	±0.15	uncleaned mixed planktonic foraminifera
9.5	3.0	0.512354	±0.000010	-5.53	±0.20	uncleaned mixed planktonic foraminifera
10	3.1	0.512357	±0.000008	-5.49	±0.16	cleaned mixed planktonic foraminifera
10	3.1	0.512360	±0.000012	-5.42	±0.23	uncleaned mixed planktonic foraminifera
10	3.1	0.512359	±0.000007	-5.44	±0.13	uncleaned mixed planktonic foraminifera
14.5	4.3	0.512358	±0.000009	-5.46	±0.18	uncleaned mixed planktonic foraminifera
18	5.1	0.512415	±0.000014	-4.36	±0.27	uncleaned mixed planktonic foraminifera
18	5.1	0.512430	±0.000013	-4.06	±0.25	uncleaned <i>G. ruber</i>
22	5.9	0.512417	±0.000009	-4.31	±0.18	uncleaned mixed planktonic foraminifera
29	6.9	0.512455	±0.000011	-3.57	±0.22	uncleaned <i>G. ruber</i>
95	8.7	0.512450	±0.000012	-3.67	±0.23	uncleaned mixed planktonic foraminifera
102	8.9	0.512471	±0.000017	-3.26	±0.33	uncleaned mixed planktonic foraminifera
102	8.9	0.512490	±0.000015	-2.89	±0.29	uncleaned <i>G. ruber</i>
120	9.1	0.512468	±0.000009	-3.31	±0.17	uncleaned mixed planktonic foraminifera
200	9.7	0.512498	±0.000009	-2.72	±0.18	uncleaned mixed planktonic foraminifera
205	9.8	0.512509	±0.000011	-2.51	±0.21	cleaned mixed planktonic foraminifera
205	9.8	0.512529	±0.000008	-2.12	±0.16	cleaning solution, mixed planktonic foraminifera
273	12.3	0.512452	±0.000012	-3.63	±0.23	uncleaned mixed planktonic foraminifera
280	12.7	0.512482	±0.000013	-3.05	±0.25	uncleaned mixed planktonic foraminifera
293	14.1	0.512450	±0.000009	-3.66	±0.17	cleaned mixed planktonic foraminifera
293	14.1	0.512474	±0.000007	-3.20	±0.14	cleaned <i>G. ruber</i>
293	14.1	0.512459	±0.000023	-3.49	±0.44	cleaning solution, mixed planktonic foraminifera
293	14.1	0.512483	±0.000017	-3.02	±0.34	cleaning solution, <i>G. ruber</i>
299	16.4	0.512398	±0.000010	-4.68	±0.19	uncleaned mixed planktonic foraminifera
303	20.6	0.512390	±0.000007	-4.83	±0.14	cleaned mixed planktonic foraminifera
303	20.6	0.512386	±0.000007	-4.91	±0.14	cleaned mixed planktonic foraminifera
315	25.8	0.512411	±0.000007	-4.44	±0.13	cleaned <i>G. ruber</i>

Table 2

Results of Nd isotopic composition obtained from planktonic foraminifera samples from core MD90-964. The age of sediments have been obtained by the correlation between the *G. ruber* $\delta^{18}\text{O}$ record and the Mediterranean *G. ruber* stack compiled by Lourens (2004) (Zhao et al., 2011).

Depth (cm)	Age (kyr)	$^{143}\text{Nd}/^{144}\text{Nd}$	$\pm 2\sigma$	ϵNd	$\pm 2\sigma$
4	0.5	0.512441	± 0.000011	-3.84	± 0.21
8	0.9	0.512413	± 0.000009	-4.39	± 0.18
16	1.9	0.512410	± 0.000008	-4.45	± 0.17
28	3.3	0.512410	± 0.000011	-4.45	± 0.21
40	4.7	0.512438	± 0.000010	-3.89	± 0.19
52	6.2	0.512454	± 0.000010	-3.58	± 0.19
72	8.5	0.512450	± 0.000011	-3.66	± 0.22
80	9.5	0.512457	± 0.000009	-3.53	± 0.18
108	13.2	0.512476	± 0.000009	-3.17	± 0.18
128	15.8	0.512430	± 0.000010	-4.07	± 0.19
152	19.0	0.512464	± 0.000009	-3.40	± 0.18
160	20.0	0.512462	± 0.000010	-3.43	± 0.19
172	22.8	0.512537	± 0.000009	-1.96	± 0.17
200	29.5	0.512470	± 0.000008	-3.27	± 0.15
224	35.2	0.512483	± 0.000008	-3.03	± 0.16
236	38.0	0.512462	± 0.000010	-3.43	± 0.19
280	45.0	0.512478	± 0.000010	-3.12	± 0.19
304	48.8	0.512474	± 0.000010	-3.20	± 0.20
324	51.9	0.512473	± 0.000009	-3.22	± 0.18
380	60.8	0.512497	± 0.000011	-2.75	± 0.21
384	61.4	0.512483	± 0.000009	-3.02	± 0.18
420	67.1	0.512484	± 0.000010	-3.00	± 0.19
452	72.1	0.512442	± 0.000010	-3.82	± 0.20
484	77.2	0.512430	± 0.000010	-4.06	± 0.20
504	80.4	0.512440	± 0.000008	-3.85	± 0.16
512	81.8	0.512456	± 0.000007	-3.55	± 0.15
524	84.3	0.512459	± 0.000008	-3.50	± 0.16
556	91.0	0.512412	± 0.000008	-4.42	± 0.15
580	96.0	0.512453	± 0.000010	-3.60	± 0.20
592	98.5	0.512455	± 0.000009	-3.58	± 0.18
596	99.3	0.512484	± 0.000010	-3.00	± 0.19
600	100.2	0.512462	± 0.000011	-3.42	± 0.22
604	101.0	0.512469	± 0.000009	-3.30	± 0.18
608	102.3	0.512495	± 0.000015	-2.79	± 0.29
628	108.7	0.512439	± 0.000009	-3.88	± 0.17
632	110.0	0.512331	± 0.000008	-5.99	± 0.39
636	110.9	0.512454	± 0.000009	-3.59	± 0.16
652	114.5	0.512431	± 0.000016	-4.03	± 0.18
656	115.4	0.512432	± 0.000010	-4.01	± 0.32
660	116.3	0.512421	± 0.000009	-4.23	± 0.19
664	117.2	0.512427	± 0.000008	-4.12	± 0.17
668	118.1	0.512415	± 0.000009	-4.35	± 0.16
672	119.0	0.512397	± 0.000010	-4.70	± 0.17
676	119.9	0.512420	± 0.000010	-4.25	± 0.20
680	120.8	0.512405	± 0.000011	-4.54	± 0.20
684	121.7	0.512429	± 0.000009	-4.07	± 0.22
688	122.6	0.512436	± 0.000009	-3.94	± 0.17
692	123.5	0.512429	± 0.000013	-4.07	± 0.18
700	128.0	0.512399	± 0.000011	-4.66	± 0.24
704	130.3	0.512421	± 0.000009	-4.23	± 0.21
708	132.5	0.512418	± 0.000012	-4.29	± 0.18
712	134.8	0.512446	± 0.000013	-3.75	± 0.23
716	137.0	0.512483	± 0.000008	-3.02	± 0.26
720	139.8	0.512448	± 0.000009	-3.71	± 0.16
728	145.4	0.512454	± 0.000011	-3.59	± 0.17

2012). These time intervals are also associated with an increase of C_{org} in core MD90-964 and are coeval with the deposition of sapropels S5 (128.0–117.7 cal kyr BP), S4 (102.3–100.6 cal kyr BP), S3 (81.8–79.7 cal kyr BP) and S1 (10.1–5.7 cal kyr BP) (Fig. 4F) (Zhao et al., 2011). In particular, ϵNd values systematically increase before the deposition of sapropels S4, S3 and S1.

For the last 20 cal kyr BP, the ϵNd record obtained on core MD90-964 displays long-term variations that are consistent with those of core MS27PT. Interestingly, higher ϵNd values from ~14 to ~6 cal kyr BP are coeval with the timing of the AHP (Fig. 3). The time interval between 9 and 6 cal kyr BP is marked by a steady decrease of ϵNd

during the Late Holocene (Fig. 3), whereas the interval between 4 and about 1.5 cal kyr BP displays lower values before they increase again during the last 1.5 cal kyr BP.

5.2. Regional compilation of seawater ϵNd of the Levantine Basin

Previous studies of the Nd isotopic compositions of authigenic oxy-hydroxides in the Levantine Basin have been conducted on leached bulk sediment (Freydier et al., 2001; Cornuault et al., 2018; Wu et al., 2019), fish debris/teeth (Wu et al., 2019) and on planktonic foraminifera (Scrivner et al., 2004; Vance et al., 2004; Osborne et al., 2010; Cornuault et al., 2018; Wu et al., 2019). Past seawater ϵNd has been obtained from bulk sediment leachates using different analytical procedures such as bulk sediment leached with 1 M HCl (Freydier et al., 2001; Wu et al., 2019) and hydroxylamine hydrochloride of non-decarbonated samples (Tachikawa et al., 2004; Cornuault et al., 2018). ϵNd analyses of foraminifera have previously been conducted on both uncleaned foraminifera (Cornuault et al., 2018) and samples treated with an oxidative-reductive leaching procedure (Scrivner et al., 2004; Vance et al., 2004; Osborne et al., 2010). All of these analytical procedures have been debated within the scientific community and have been deemed suitable for extracting the ϵNd signature of the deep-water masses of the ocean.

Previous ϵNd records based on cleaned foraminifera collected in the eastern Levantine Basin (ODP Site 967C - 34°04.270'N; 32°43.528'E; 2552.8 m; Scrivner et al., 2004), in the western Levantine Basin (ODP Site 971A - 33°42.818'N; 24°42.108'E; 2140.9 m; Osborne et al., 2008) and in the south-eastern Aegean Sea (core LC21 - 35°39.7'N; 26°35.0'E; 1520 m; Osborne et al., 2010) were used to reconstruct past ϵNd of surface waters. However, it has been recently demonstrated that ϵNd of fossil planktonic foraminifera is not related to the ambient seawater at calcification depths, but instead reflects bottom and/or pore-water ϵNd values due to the presence of residual authigenic Fe–Mn coatings precipitated onto the carbonate shells that cannot be removed by chemical cleaning procedures (Piotrowski et al., 2012; Roberts et al., 2012; Wu et al., 2015b; Xu et al., 2018). ϵNd results obtained from cleaned foraminifera of core LC21 and ODP sites 967C and 971A should be interpreted as bottom/pore water ϵNd .

ODP Site 967C is also located within the EMDW (2551 m) and about 100 km away from core MD90-964 making it possible to directly compare their ϵNd records for time intervals corresponding to sapropels S1 and S5 (Figs. 5 and 6). ϵNd records for core MD90-964 and Site 967C, display more radiogenic values during African Humid Periods than before and after these time intervals. For core MD90-964, the highest ϵNd value is observed in the early African Humid Period (at 13.2 cal kyr BP) before the deposition of sapropels S1. Except this highest ϵNd value, both sapropels of core MD90-964 (S5 and S1) display a range from -3.5 ± 0.2 to -4.8 ± 0.2 , characterized by slightly more radiogenic values compared to those obtained in the ODP Site 967C (-5.5 ± 0.5 to -3.1 ± 0.2 ; Scrivner et al., 2004).

For the last 20 cal kyr BP, core MS27PT is also characterized by similar long-term variations of ϵNd with an interval of more radiogenic values between 14 and 6 cal kyr BP followed by a progressive return to unradiogenic values from 6 to 4 cal kyr BP. For cores MS27PT and MD90-964, the last about 1.5 cal kyr BP show more radiogenic values. The good agreement observed in the long-term changes of the ϵNd during the S5 (for core MD90-964 and ODP Site 967C) and the last 18 cal kyr BP (for core MS27PT, core MD90-964 and ODP Site 967) suggests that all these cores provide a regional Nd isotopic signature of the EMDW.

Core MD04-2722 located south of Cyprus at 1780 m water depth in the eastern Levantine Basin (Fig. 1) presents radiogenic LGM ϵNd

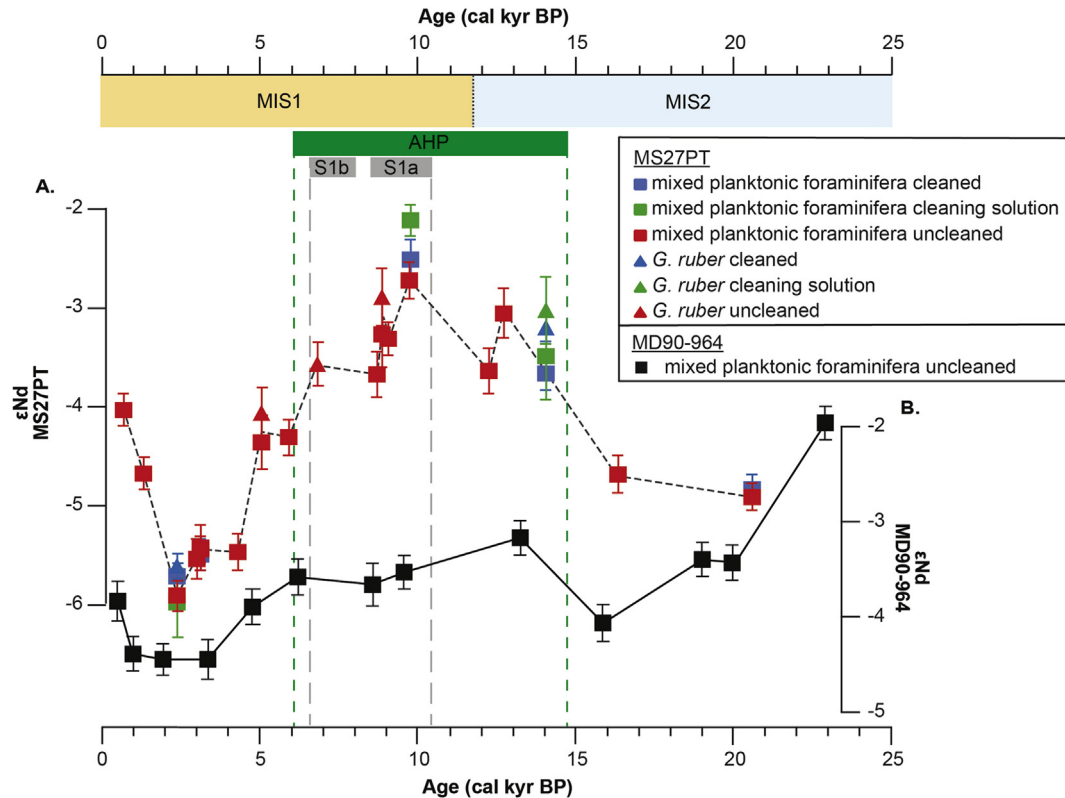


Fig. 3. (A) Nd isotopic composition (ϵ_{Nd}) obtained from foraminifera of core MS27PT: ϵ_{Nd} values obtained from cleaning solution of *G. ruber* (solid green triangle), reductively cleaned *G. ruber* (solid blue triangle), non-reductively cleaned *G. ruber* (solid red triangle), reductively cleaned mixed planktonic foraminifera (solid blue rectangle), cleaning solution of mixed planktonic foraminifera (solid green rectangle), non-reductively cleaned mixed planktonic foraminifera (solid red rectangle); (B) ϵ_{Nd} obtained on non-reductively cleaned mixed planktonic foraminifera (solid black square) of core MD90-964 for the last 23 cal kyr BP. The Marine Isotope Stages (MIS) and time intervals of sapropel S1 and AHP are also reported. (For interpretation of the references to color in this figure legend, the reader is referred to the Web version of this article.)

values (around -3), comparable to those observed for cores located along the Nile deep-sea fan. ϵ_{Nd} values decrease between 17.5 and 15 cal kyr BP followed by a time interval characterized by radiogenic isotopic composition between 14.5 and 5 cal kyr BP (Fig. 5). The time interval thereafter (between 5 and 3 cal kyr BP) is associated with a slight decrease in the ϵ_{Nd} values. Such long-term variations in ϵ_{Nd} are quite similar to those observed in cores MD90-964 and MSPT27 located upstream of the general counter-clockwise deep-sea circulation of the eastern Mediterranean basin (Fig. 1). Superimposed on this long-term trend, core MD04-2722 is characterized by shifts of ϵ_{Nd} to unradiogenic values around 13.5 and 6.8 cal kyr BP that are not observed in other ϵ_{Nd} records of the Levantine Basin (MD90-964, MS27PT and ODP Site 967C), with the exception of one shift to a single unradiogenic value at 6.8 cal kyr BP which is also observed in the ODP Site 967C (Fig. 5). This may reflect different time resolutions or a potential local effect on Nd isotopic signature. This implies that long-term variations of ϵ_{Nd} below approximately 1300 m water depth reflect a regional ϵ_{Nd} signal of the Levantine Basin. We note a slight decrease of the ϵ_{Nd} range along the north-eastward circulation pattern of the deep-water masses that could be the result of a slight modification of the Nd isotopic signature of deep-water masses through lithogenic Nd input from the volcanic margin of the eastern Levantine Basin.

In contrast, the ϵ_{Nd} record of core BC07, located closer to core MD90-964 and at shallower depth (893 m), displays variations from -6.2 ± 0.3 to -4.2 ± 0.3 (Freydier et al., 2001) that differ somewhat from those of ODP Site 967C and core MD90-964 during the AHP (Fig. 5). While time intervals before 15 cal kyr BP and after

6 cal kyr BP are characterized by similar ϵ_{Nd} variations as ODP Site 967C and cores MD90-964 and MS27PT, the AHP is instead associated with more unradiogenic ϵ_{Nd} , with values as low as -5.9 ± 0.3 during the sapropel S1. This suggests that the ϵ_{Nd} record of water masses at ~ 900 m differs from those obtained at greater water depths (below ~ 1300 m) for a time interval between 14 and 6 cal kyr BP. The difference between ϵ_{Nd} records above and below ~ 1300 m reaches its maximum during the time interval of sapropel S1 deposition.

6. Discussion

The ϵ_{Nd} record obtained from uncleaned foraminifera of core MD90-964 allows us to establish, for the first time, the Nd isotopic signature of the EMDW of the Levantine Basin over the last climatic cycle and to extend our knowledge of the ϵ_{Nd} variability for sapropels S1 and S5 to those of S3 and S4. The ϵ_{Nd} record of core MD90-964 also displays glacial-interglacial variability with more radiogenic values during glacial MIS (Fig. 4).

A prerequisite for interpreting such seawater ϵ_{Nd} variations through time is the characterization of present-day and past Nd isotopic composition of the main water masses circulating in the eastern Mediterranean basin. Thus, we can evaluate potential temporal changes in the ϵ_{Nd} of the end-members during the last climatic cycle, and assess the potential influences of lithogenic Nd input and regional “boundary exchange” on ϵ_{Nd} of deep-water masses.

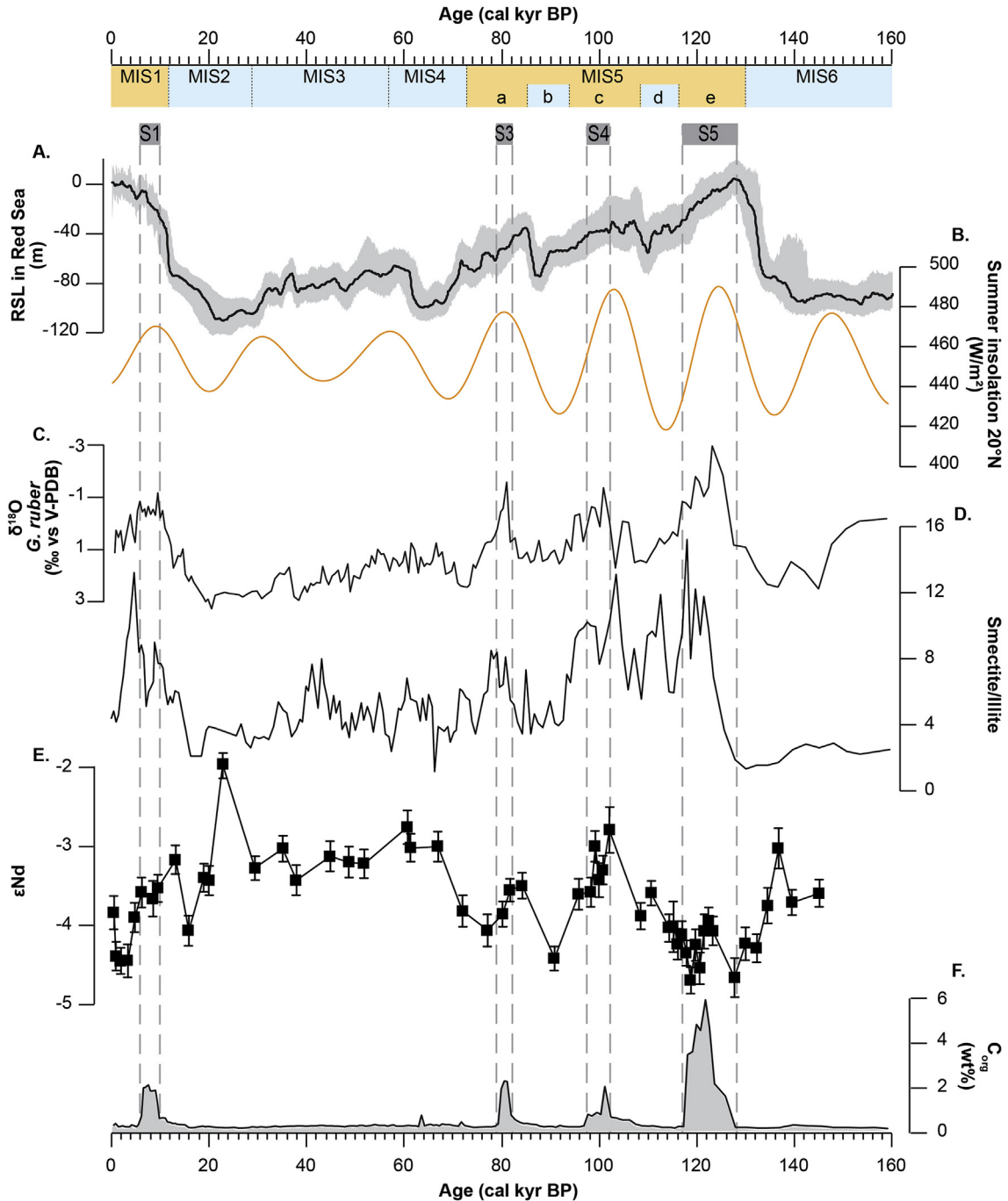


Fig. 4. Variations in (A) the Relative Sea Level (RSL) (Grant et al., 2014) and (B) the summer insolation (June and July) received by the Earth at 20°N, calculated using Analseries software (Paillard et al., 1996) for the last 160 kyr. (C) Variations of the $\delta^{18}\text{O}$ obtained from *G. ruber* of core MD90-964 (Zhao et al., 2011); (D) Variations of the smectite/illite ratio of core MD90-964 (Zhao et al., 2011); (E) Variations of the Nd isotopic composition (ϵNd) obtained from uncleaned mixed planktonic foraminifera of core MD90-964 (this study); (F) Variations of the Total Organic Carbon (wt%) of sediments from core MD90-964 (Zhao et al., 2011). The Marine Isotope Stages (MIS) and time intervals of Sapropel S1 to S5 deposition are also reported.

6.1. Possible impact of changes in lithogenic Nd input on the ϵNd of the Eastern Mediterranean Deep Water in the Levantine Basin

At the present time, the EMS is characterized by contrasting seawater ϵNd values (~ -10 to ~ -5) with strong zonal and vertical gradients which are attributed to a mixing between the inflowing MAW (~ -10) and the more radiogenic underlying LIW (~ -5) and EMDW (~ -6.5) (Tachikawa et al., 2004) (Fig. 1b). The latter acquires its ϵNd signature from boundary exchange with radiogenic basaltic

material originating from the Ethiopian traps, which is transported to the EMS by the Nile river ($\epsilon\text{Nd} = -3$ to $+3$, Tachikawa et al., 2004), and from the volcanic arc of the Aegean Sea ($\epsilon\text{Nd} \sim -2.5$), with the most radiogenic material being located at the eastern border of the Levantine Basin ($\epsilon\text{Nd} = +3.5$ to $+6$) (Ayache et al., 2016).

In this regard, previous studies have explored past variations of seawater ϵNd in the Levantine Basin as a balance between unradiogenic aeolian Saharan dust and radiogenic Nile river discharge

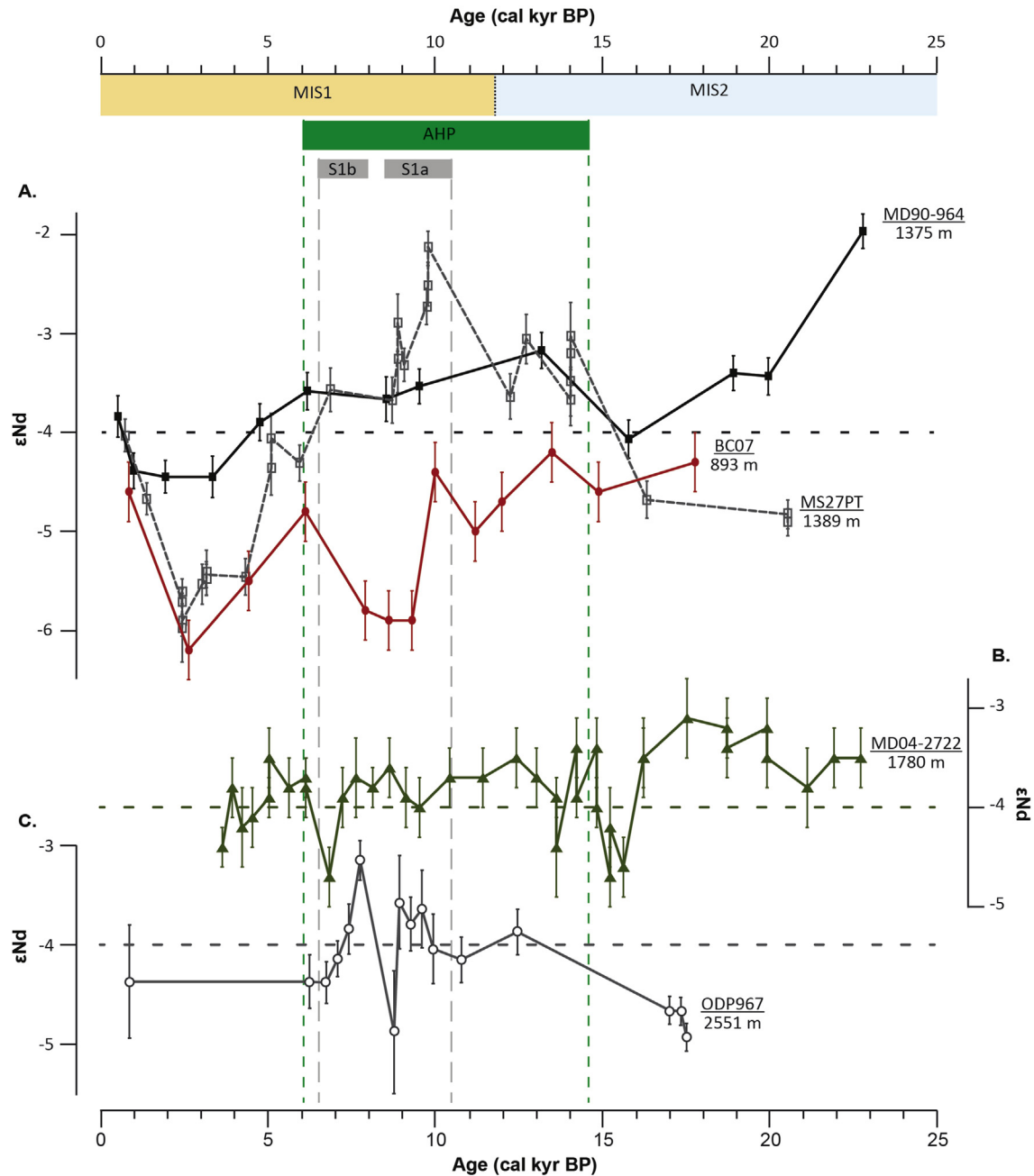


Fig. 5. Comparison between ϵNd records obtained in this study (cores MD90-964 and MS27PT) and published records for the last 25 kyr. Core MD04-2722: Cornuault et al. (2018); core BC07: Freyrier et al. (2001) ODP Site 967C: Scrivner et al. (2004).

(Scrivner et al., 2004; Revel et al., 2015; Cornuault et al., 2018; Wu et al., 2019), including the possibility of a significant contribution from paleo-rivers along the African margin (Osborne et al., 2010), or a predominant contribution through the mechanism of boundary exchange (Ayache et al., 2016; Vadsaria et al., 2019; Wu et al., 2016). Tachikawa et al. (2004) have suggested that the Nd flux from Nile River freshwater has a minor influence on the present-day Mediterranean seawater ϵNd , with its Nd concentration being low and the water input 10 times smaller than the unradiogenic AW flowing from the Western Basin to the shallow waters of the Levantine Basin. Several previous studies have demonstrated that detrital material in the Nile deep-sea fan results from the mixing of sediments derived from Saharan/Libyan dusts and Nile sediments (Weldeab et al., 2002a; Scheuven et al., 2013; Garzanti et al., 2015;

Revel et al., 2015). Cores MD90-964 and MS27PT, located on the Nile deep-sea fan, are then suitable for assessing lithogenic Nd input to the EMDW.

6.1.1. Contribution of the Nile river

Past humid periods, corresponding to the sapropels, were systematically accompanied by higher deposition of iron/smectite-rich sediments in the Nile deep-sea fan, reflecting enhanced physical erosion and transport of sediments from the Ethiopian Highlands (Krom et al., 1999, 2002; Weldeab et al., 2002b; Revel et al., 2010, 2014, 2015; Langgut et al., 2011; Zhao et al., 2012). In contrast, past arid periods are associated with a lower contribution from the Blue Nile and a higher relative proportion of sediments derived from the White Nile, along with a peak in the aeolian dust component (Revel

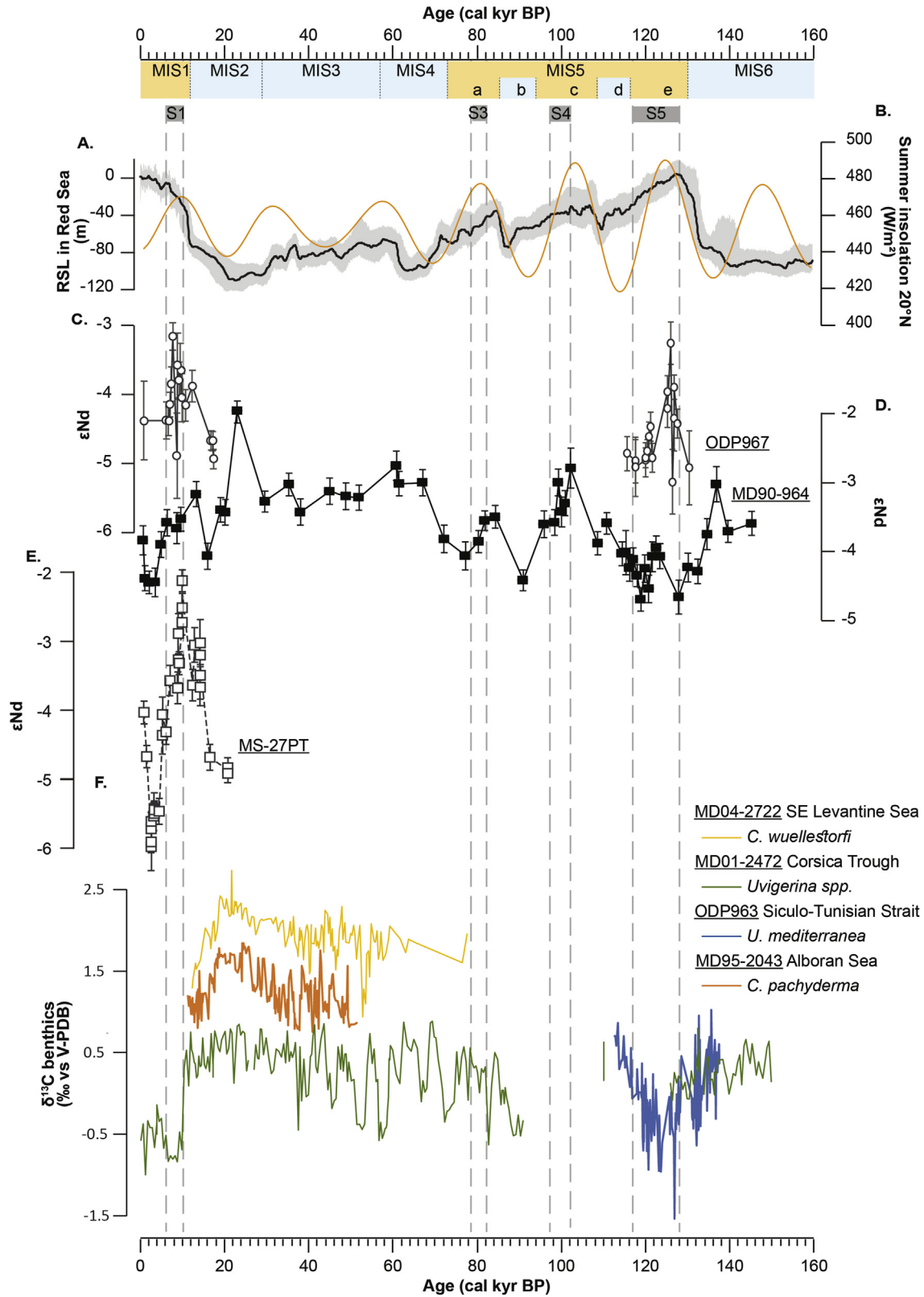


Fig. 6. (A) Variations in Relative Sea Level (RSL) (Grant et al., 2014); (B) summer insolation (June and July) received by the Earth at 20°N, calculated using Anlseries software (Paillard et al., 1996) for last 160 kyr. (C) εNd record obtained from ODP Site 967C (Osborne et al., 2010); (D) εNd record obtained from non-reductively cleaned mixed planktonic foraminifera of core MD90-964 (this study); (E) εNd record obtained from non-reductively cleaned mixed planktonic foraminifera of core MS27PT (this study); (F) compilation of δ¹³C obtained from benthic foraminifera from Mediterranean cores. Records of δ¹³C obtained from benthic foraminifera are published as followed: MD04-2722 by Cornuault et al. (2016); MD01-2472 by Toucanne et al. (2012); ODP Site 963 by Incarbona et al. (2011); MD95-2043 by Cacho et al. (2000).

et al., 2015; Zhao et al., 2012). Large smectite contents recorded in cores MD90-964 (Zhao et al., 2012) (Fig. 4D) and MS27PT, combined with Sr and Nd isotopic compositions (Revel et al., 2014) indicate the dominant contribution of the Blue Nile (smectite) to the Nile discharge, at least during the last climatic cycles. The low proportion of sediment derived from the White Nile is mainly due to the Sudd marshes in Southern Sudan which efficiently trap sediments from tributaries of the White Nile (Padoan et al., 2011; Garzanti et al., 2015). In addition, during the African Humid Periods, it has been suggested that large lakes formed in the region extending from Sudd to the confluence at Khartoum (Barrows et al., 2014). These lakes likely further limited the northward transport of unradiogenic Nd sediments to the Nile deep-sea fan. Thus, there is no argument to support the hypothesis that changes in the relative contribution of the Equatorial-White Nile and Blue Nile tributaries triggered the seawater ϵNd variations observed in cores MD90-964 and MSPT27.

6.1.2. Contribution of African dust

The Saharan dust transported to the EMS is characterized by an unradiogenic ϵNd values (-15 to -11 ; Padoan et al., 2011; Scheuven et al., 2013), potentially contributing to the unradiogenic Nd isotopic signature of surface and intermediate water masses (e.g. Tachikawa et al., 2004; Ayache et al., 2016). However, the present-day distribution of ϵNd in the surface and intermediate water masses of the Mediterranean Sea is mainly attributed to the mixing of the AW and the LIW and suggests a negligible contribution of Nd lithogenic input from aeolian dusts (Wu et al., 2019).

In addition, core MD90-964, located at a distal position on the deep-sea fan, is characterized by lower mean sedimentation rates (5 cm/kyr) compared to core MS27PT (12 cm/kyr) and may be associated with a higher proportion of Saharan dust components. Variations in the mineralogical ratio of smectite/illite obtained on the clay fraction of core MD90-964 have been used to track the relative proportions of Saharan dust (characterized by high illite contents) and Nile contributions (dominated by smectite, 90%, derived from the Blue Nile and Atbara River draining the Ethiopian Plateau flood basalts) (Zhao et al., 2011) (Fig. 4D). The transport of Saharan dust to the Levantine Basin, reconstructed from the smectite/illite ratio, displays slight glacial-interglacial variations with elevated dust inputs during glacial periods. Such results are in agreement with previous studies reporting an increase in dust input to the Mediterranean Sea during this time span induced by the southward migration of the ITCZ (Weldeab et al., 2002b; Revel et al., 2010; Ehrmann et al., 2016, 2017; Lamb et al., 2018) (Fig. 4D). Such glacial increases of unradiogenic ϵNd dust inputs to the eastern Mediterranean Basin do not appear to have significantly modified the seawater ϵNd record obtained in core MD90-964, since glacial periods (MIS6 and MIS2-4) are systematically associated with more radiogenic ϵNd values than those of interglacial periods (MIS5 and MIS1) (Fig. 4D and E).

In addition, the seawater ϵNd record obtained in core BC07, which was collected at a shallower depth (893 m), could have been slightly more affected by the dissolution of Saharan dust relative to the other deeper cores. Such higher contribution of dust dissolution in the upper water column has been demonstrated in previous studies (e.g. Ayache et al., 2016). Yet, this core does not exhibit variations in seawater ϵNd that might have been induced by a glacial increase in dust fluxes. The time interval corresponding to the AHP (from ~ 14.8 to ~ 6 cal kyr BP), when a decrease of aeolian dusts has been demonstrated (DeMenocal et al., 2000; Ehrmann et al., 2013), is in fact associated with more unradiogenic ϵNd (Fig. 5). A negligible contribution of the dissolution of African dust on past seawater ϵNd since the last glacial period has been also proposed by Cornuault et al. (2018) and Wu et al. (2019) for several

seawater ϵNd records obtained from cores located between ~ 800 and ~ 3400 m water depth in the western part of the EMS.

6.1.3. Contribution of African paleo-rivers

A vast fossil river channel network has been identified in the Libyan Sahara, which was active during African Humid Periods (Rohling et al., 2002). These paleo-rivers carried alteration products originating from basalts of the Tibesti mountains, ($\epsilon\text{Nd} = 5$ to 7 ; Allegre et al., 1981). Some lake mollusks analyzed in Wadi Behar Belema and Wadi Quoquin (two of these paleo-rivers) have shown that the freshwater was significantly radiogenic ($\epsilon\text{Nd} = -2.2$ to -1.8) compared to the Saharan dust (Osborne et al., 2008). Therefore, it has been suggested that these Libyan paleo-rivers contributed an additional source of radiogenic Nd to the eastern Mediterranean Basin during African Humid Periods (Scrivner et al., 2004). Seawater ϵNd records for core ODP site 971A (proximal to the mouths of these paleo-rivers compared to more distal ODP Site 967C or core LC21), were used to support this hypothesis during sapropel S5 (Osborne et al., 2008, 2010). However, for different reasons, variations in the foraminiferal ϵNd obtained from cores located in the eastern EMS cannot be entirely explained by changes in the Nd isotopic composition of the water masses induced by lithogenic input from the African paleo-rivers. First, Sr and Nd isotopic signatures of the detrital fraction of sediments close to the mouth of these Libyan paleo-rivers (core CP10BC), have shown maximum sediment discharges during the sapropel S1b time interval (Wu et al., 2016) whereas ϵNd records display more radiogenic values at the beginning of the AHP (~ 14.8 cal kyr BP), reaching a maximum at ~ 13.5 cal kyr BP for core MD90-964 and at ~ 9.7 cal kyr BP for core MS27PT (Fig. 5). Second, the sapropel time interval in cores MD90-964 and MS27PT, as well as in several cores previously investigated throughout the EMS (Wu et al., 2019), is associated with a continuous decrease in ϵNd values during the deposition of sapropel S1 indicating a more radiogenic signature for the S1a than for the S1b time interval (Fig. 5). Finally, core CP10, which should be susceptible to a significant influence from the discharge of Libyan paleo-river sediments due to its proximal location does not in fact exhibit any influence on its seawater ϵNd record (Wu et al., 2019). Therefore, while we cannot fully rule out a local influence of detrital discharge from the Libyan paleo-rivers on seawater ϵNd , its contribution to Levantine deep-water masses can be considered negligible.

In conclusion, the process of “boundary exchange” between water masses and volcanic sediment along the margin of the eastern and northern Levantine Basin is one of the major sources of lithogenic Nd to the Mediterranean Sea (Ayache et al., 2016), but neither changes in the inputs of lithogenic Nd from the Nile River nor from the paleo-rivers of the North African margin can explain the glacial-interglacial variability observed in the seawater ϵNd records of core MD90-964.

6.2. Paleo-hydrological implications of the ϵNd records during glacial-interglacial transitions and terminations I and II

The ϵNd records for the EMS display significant glacial and interglacial variations, ranging from -2.0 ± 0.2 to -4.3 ± 0.2 , with more radiogenic values during glacial MIS6, 4, 3 and 2 (Fig. 4) that may have been induced by the result of an increase in the residence time of deep-water masses in the EMS and/or a decrease in the proportion of unradiogenic MAW flowing into the EMS.

Using a regional ocean-atmosphere coupled climate model, Vadsaria et al. (2019) have shown that a reduction in the formation of deep water in the Eastern basin is associated with an increase in deep-water ϵNd due to a longer interaction between the water masses and the radiogenic sediments along the eastern margins of

the EMS (Ayache et al., 2016). However, since the ventilation of the EMDW was enhanced during glacial MIS2, 4 and 6, due to saltier and denser surface water (Thunell and Williams, 1989; Béthoux et al., 1990; Myers et al., 1998a), the more radiogenic ϵNd values for the EMDW during glacial periods cannot be attributed to a modification of the residence time of deep-water masses. Moreover, several models have shown that exchange between the Atlantic Ocean and the Mediterranean Sea may have been reduced by as much as half during the glacial low sea-level stands, resulting in a higher longitudinal salinity gradient in the Mediterranean Sea (Bryden et al., 1994; Myers et al., 1998b; Mikolajewicz, 2011; Grimm et al., 2015). Periods of glacial low sea level may have caused a 50% reduction in water exchange between the eastern and the western Mediterranean basins through the Sicilo-Tunisian Strait (Mikolajewicz, 2011; Grimm et al., 2015). Consequently, taking into account that glacial periods were associated with enhanced convection of deep water in the EMS, the more radiogenic ϵNd observed for the glacial EMDW can be attributed to a decrease in the contribution of the Modified Atlantic Water (MAW) to the eastern Mediterranean Basin. In this case, therefore, there is an entrainment of radiogenic ϵNd surface water to the deep basin at the center of production of deep-water masses. However, we cannot exclude that the decrease in zonal water exchange between the WMS and the EMS during the glacial period favored also a longer contact time between the EMDW and the radiogenic sediment draping the eastern Mediterranean continental margin during this time. This hypothesis would need to be tested further using a regional modeling approach.

However, we have tried to estimate the reduction of MAW to the EMS necessary to explain an increase of 1.5 ϵNd unit observed in core MD90-964 during glacial time relative to the low values of the MIS1 and 5 (out of sapropel and African Humid Periods) using a simple box-model for Nd in the EMS established by Wu et al. (2019). We have used the present-day input of Nile river and dust to the EMS (Nile \times 1, Dust \times 1; Fig. 5 of Wu et al., 2019). Results suggest that the observed glacial increase of ϵNd could be attributed to a decrease of MAW by 55% relative to today. Such variations are likely overestimated as the radiogenic Nd contribution from Nile could have also been reduced during glacial period. Nevertheless, the calculated reduction of MAW inflow into the EMS during glacial low sea-level stands agrees with the 50% reduction in water exchange between the eastern and the western Mediterranean basins through the Siculo-Tunisian Strait quantified by Mikolajewicz (2011) for the LGM.

The ϵNd record of core MD90-964 covers the last Terminations I and II. The significant decrease in the ϵNd value (from -3.2 ± 0.2 to -4.4 ± 0.2) during Termination I begins at around 18 cal kyr BP and is coeval with a similar decrease in $\delta^{13}\text{C}$ obtained from benthic foraminifera (Incarbona et al., 2011; Sprovieri et al., 2012; Toucanne et al., 2012; Cornuault et al., 2016) (Fig. 6). The decrease of the ϵNd during Termination II observed in core MD90-964 is also associated with a decrease of benthic $\delta^{13}\text{C}$, which is particularly well marked in the Ionian Basin, close to the Siculo-Tunisian Strait (Incarbona et al., 2011). The decrease in $\delta^{13}\text{C}$ obtained on benthic foraminifera has been linked to a reduction in deep-water convection in the Mediterranean Sea, but the influence of an increase in surface productivity cannot be excluded (Incarbona et al., 2011; Cornuault et al., 2016). During both terminations, the decrease in ventilation suggested by the benthic foraminifera $\delta^{13}\text{C}$ record is not associated with more radiogenic values, as expected if the seawater residence time in the EMS had increased. On the contrary, the ϵNd record shows a decrease suggesting a higher contribution of unradiogenic AW to the Eastern Basin linked to the rise of the relative sea level and enhanced water mass exchange between the eastern and western Mediterranean basins. The timing of reduced ventilation

and increase in Atlantic Water contribution to the eastern Mediterranean basin is consistent with the ocean-biogeochemical model results obtained by Grimm et al. (2015), which indicate that deep-water anoxia requires a long prelude of deep-water stagnation of about 6 kyr, with no particularly strong eutrophication. The timing and duration of the stagnation prelude agree with the mechanisms for ORL1 (organic-rich layer) deposition in the western Mediterranean Sea proposed by Sierro et al. (2005).

In particular, the decreases in both benthic $\delta^{13}\text{C}$ and ϵNd before the sapropels S1 and S5 are coeval with the end of Heinrich Stadial 1 and 11 (HS1 and HS11), respectively. It has been postulated that an enhanced inflow of less salty seawater in the Mediterranean Sea during the HS1 time interval favored a reduction in deep-water convection in the western basin and caused the ORL1 deposition between 14.5 and 8.2 cal kyr BP (Cacho et al., 2002; Martinez-Ruiz et al., 2003). However, this time interval is still associated with deep-water convection allowing the transfer of unradiogenic ϵNd from MAW to the EMDW at the center of deep-water production in the EMS. Our new ϵNd record from core MD90-964 suggests similar mechanisms during Termination II, with a potential reduction in the salinity of the Atlantic Water flowing into the Mediterranean Sea during the HS11 (Kandiano et al., 2014; Jiménez-Espejo et al., 2015; Grant et al., 2016) and an increase in the proportion of MAW in the deep-water masses of the EMS, 5–6 kyr prior to the deposition of sapropel S5.

6.3. Variability of the EMS during the African Humid Periods

The ϵNd record of core MD90-964 reveals that African Humid Periods (maximum of summer insolation) of the last climatic cycle are generally associated with more radiogenic ϵNd values of the EMDW (Fig. 4). The sample from core MS27PT dated at \sim 9.7 cal kyr BP displays the most radiogenic ϵNd value (-2.5 ± 0.2), which corresponds to the maximum of summer insolation received by the Earth at 20°N (Figs. 4 and 6). The planktonic foraminifera $\delta^{18}\text{O}$ record from core 9509, located under the River Nile plume in the southeastern Levantine Basin (Fig. 1) (Almogi-Labin et al., 2009), shows the most negative values (-1‰) at \sim 9.3 cal kyr BP, suggesting a large input of freshwater from the Nile during this time. Such variations may therefore involve (i) a more efficient exchange of Nd from seawater and river sediment plumes associated with an intensification of the Nile River sediment discharge during the African Humid Periods (Revel et al., 2010; Cornuault et al., 2016) and/or (ii) a longer residence time of water masses in the EMS during time intervals of stratification of the water column that could have led to increased boundary-exchange processes at the continental margin (Lacan and Jeandel, 2005).

Recent studies have shown that river sediment discharges can modify the Nd isotopic composition of surrounding water masses (Singh et al., 2012; Chen et al., 2013; Goswami et al., 2014; Osborne et al., 2014; Rousseau et al., 2015; Wu et al., 2015a), as recently observed in the Bay of Bengal for a water depth greater than 2000 m (Yu et al., 2018). However, the ϵNd values of core BC07, collected at a shallower water-depth (893 m) in the lower portion of the LIW, are less radiogenic by 2 ϵNd units during the sapropel S1 time interval relative to the other ϵNd records available nearby (core MD90-964). This suggests that lithogenic Nd from Nile river sediment plumes did not play a major role in ϵNd variations of intermediate and deep-water masses in the eastern Mediterranean Basin during the African Humid Period. However, Nile river sediment plumes could partially explain the ϵNd variations during the deposition of sapropel S1 given that core MS27PT, located closer to the Nile river mouth, is characterized by higher ϵNd amplitude compared to what observed in core MD90-964.

Results from the recent regional circulation model developed by

Vadsaria et al. (2019), using a five-fold increase in Nile runoff during the deposition of sapropel S1, show more radiogenic ϵNd values (by 2 ϵNd units) for the deep-water masses below 1200 m, associated with a sluggish circulation, stagnation of deep water and consequent longer interaction with the surrounding radiogenic margins. This result agrees well with ϵNd records obtained for sapropels S1 to S5 (cores MS27PT and MD90-964) that display an increase of up to 2.5 ϵNd units (Figs. 5 and 6). In addition, the less radiogenic values observed in core BC07 during sapropel S1 are also consistent with model results for intermediate waters (near the LIW) (Vadsaria et al., 2019). Modeling outputs have shown a modification of the sea surface circulation pattern favorable to the propagation of unradiogenic western Mediterranean Sea waters into the intermediate waters of the Levantine Basin. The resulting ϵNd decrease observed at intermediate water depth is related to less vigorous circulation that also induces a reduction of the exchange with high-radiogenic material from the east of the EMS. Consequently, distinct variations of ϵNd records for intermediate- and deep-waters observed in cores BC07 and MD90-964 during the interval of sapropel S1 deposition are supported by models and suggest deep-water stagnation and less vigorous circulation of the LIW.

The ϵNd record of core MS27PT shows an increase around 4 kyr before the deposition of sapropel S1 (from 10.5 to 6.5 cal kyr BP, Bar-Matthews et al., 2000). This is in agreement with the recent Nile sediment discharge records that indicate an increasing discharge at ~15 cal kyr BP that could have induced a freshening of the Mediterranean Sea and a slow-down of the circulation (Revel et al., 2010). Our new results allow us to investigate the potential for a time lag between seawater ϵNd rise and sapropel onset for the previous sapropels S3, S4 and S5. The smectite/illite mineralogical ratio of core MD90-964 (Fig. 4) enables estimating the Nile discharge over the last climatic cycle (Zhao et al., 2011). This mineralogical ratio increases at about 15 cal kyr BP, in agreement with an intensification of Nile river discharge prior to the deposition of sapropel S1 (Revel et al., 2010). Taking into consideration the relatively low time resolution of the record, similar time lags can be observed between the seawater ϵNd record and the deposition of sapropels S3 and S4 (Fig. 4). The seawater ϵNd values systematically increase before the intervals of sapropels deposition but these shifts to more radiogenic values are not always associated with variations in the smectite/illite ratio. The lower time resolution of the ϵNd record of core MD90-964 around sapropel S5 does prevent us from clearly identifying a similar time lag.

The time interval coeval with sapropel S5 is characterized by lower ϵNd values relative to those of sapropels S1 and S4, and to a lesser extent to those of sapropel S3. ODP Site 967C, which is at a more distal position relative to the Nile River mouth, also displays comparable ϵNd values during the S5 mid-point, with slightly less radiogenic values (of about 0.5 ϵNd units) at the limits of S5 (Fig. 6). African monsoon rainfall has been more intense during the time interval of the S5 deposition than during sapropels S1 or S4 (Bar-Matthews et al., 2000), likely leading to more intense Nile sediment and freshwater discharges. The lower $\delta^{18}\text{O}$ *G. ruber* values obtained from core MD90-964 during S5 compared to S1 points to a more significant freshwater discharge from the Nile to the studied site (Fig. 2C). This suggests that the higher contribution of unradiogenic MAW in this period of particularly high relative sea level (Fig. 6A), may have overtaken the influence of an increase in radiogenic Nd from the Nile input and/or of a lesser vigorous deep-water circulation in the EMS during the deposition of sapropel S5. This would explain why the development of sapropel S5 is not related to higher ϵNd values compared to other sapropels, such as

S1 and S4. For sapropel S4, the ϵNd record may indicate enhanced Nile river discharge, or more likely, a reduction in EMS-WMS exchange induced by lower sea level during MIS5c compared to MIS5e (Fig. 6A). Further modeling studies are needed to estimate the relative contribution of the MAW to the eastern Mediterranean Basin under the environmental conditions prevailing during the different sapropel depositions and particularly during the high sea-level of S5.

7. Conclusions

Based on the foraminiferal ϵNd record of cores MD90-964 and MS27PT, located in the eastern Levantine Basin, we provide evidence of significant glacial-interglacial variations in the inflow of Atlantic Water to the EMS during the last climate cycle (last 145 kyr). We have demonstrated for the first time that ϵNd values for the EMDW are systematically associated with more radiogenic values during glacial Marine Isotope Stages. Such long-term glacial to interglacial variations in ϵNd values cannot be solely the result of changes in Nile river discharge and Saharan dust inputs. Decreases in ϵNd values during MIS5 and MIS1 interglacials have been attributed to an increase in the contribution of unradiogenic MAW to the EMS related to high sea-level stands and enhanced seawater exchange between the North Atlantic and the Mediterranean basins. Termination I and II are associated with a decrease in seawater ϵNd in line with a decrease in the $\delta^{13}\text{C}$ obtained from benthic foraminifera, suggesting a sluggish deep-sea ventilation in the EMS related to a higher contribution of Atlantic Water in the EMS through the Siculo-Tunisian Strait during sea-level rise.

Superimposed on this long-term glacial-interglacial variation, a monsoon–precession induced signal is distinguished in ϵNd records by more radiogenic values related to African Humid Periods (and sapropel events). These periods of radiogenic ϵNd of the EMDW have been associated with an intensification of Nile discharge and an increase in the residence time of deep-water masses in the EMS, leading to an increase in the contact time between deep-water masses and radiogenic sediments along the continental margin of the EMS.

Overall, our ϵNd records combined with previous ϵNd values obtained in the EMS reinforce the hypothesis that a drastic reduction in the hydrological exchanges between the western and eastern Mediterranean basins, and a subsequent higher proportion of Atlantic Water during sea level rise may have preconditioned sapropel deposition in the EMS during the last climatic cycle, as proposed by Grimm et al. (2015).

Declaration of competing interest

The authors declare that they have no known competing financial interests or personal relationships that could have appeared to influence the work reported in this paper.

Acknowledgements

The research leading to this paper was funded by the French National Research Agency under the “Investissements d’avenir” programme (Grant ANR-11-IDEX-0004-17-EURE-0006), the HAMOC Project (Grant ANR-13-BS06-0003) and the INSU LEFE-IMAGO PALMEDS Project. We gratefully acknowledge the support provided by Louise Bordier during Nd isotopic composition analyses. We especially thank Adi Torfstein and an anonymous reviewer for their constructive reviews, which significantly helped to improve this manuscript.

References

- Allegre, C.J., Dupré, B., Lambert, B., Richard, P., 1981. The subcontinental versus suboceanic debate. Lead-neodymium-strontium isotopes in primary alkali basalts from a shield area, the Ahaggar volcanic suite. *Earth Planet Sci. Lett.* 52, 85–92.
- Allen, J.R.M., Huntley, B., Brandt, U., Brauer, A., Hubberten, H., Keller, J., Kraml, M., Mackensen, A., Mingram, J., Negendank, J.F.W., Nowaczyk, N.R., Oberhänsli, H., Watts, W.A., Wulf, S., Zolitschka, B., 1999. Rapid environmental changes in southern Europe during the last glacial period. *Nature* 400, 740–743. <https://doi.org/10.1038/23432>.
- Almogi-Labin, A., Bar-Matthews, M., Shriki, D., Kolosovsky, E., Paterne, M., Schilman, B., Ayalon, A., Aizenshtat, Z., Matthews, A., 2009. Climatic variability during the last ~90 ka of the southern and northern Levantine Basin as evident from marine records and speleothems. *Quat. Sci. Rev.* 28, 2882–2896. <https://doi.org/10.1016/j.quascirev.2009.07.017>.
- Angue Minto'o, C.M., Bassetti, M.A., Morigi, C., Ducassou, E., Toucanne, S., Jouet, G., Mulder, T., 2015. Levantine intermediate water hydrodynamic and bottom water ventilation in the northern Tyrrhenian Sea over the past 56,000 years: new insights from benthic foraminifera and ostracods. *Quat. Int.* 357, 295–313. <https://doi.org/10.1016/j.quaint.2014.11.038>.
- Arbuszewski, J.A., Demenocal, P.B., Cléroux, C., Bradtmiller, L., Mix, A., 2013. Meridional shifts of the Atlantic intertropical convergence zone since the last glacial maximum. *Nat. Geosci.* 6, 959–962. <https://doi.org/10.1038/ngeo1961>.
- Ayache, M., Dutay, J.-C., Arsouze, T., Révillon, S., Beuvier, J., Jeandel, C., 2016. High resolution neodymium characterization along the Mediterranean margins and modeling of ϵ_{Nd} distribution in the Mediterranean basins. *Biogeosci. Discuss.* 1–31. <https://doi.org/10.5194/bg-2016-109>.
- Bar-Matthews, M., Ayalon, A., Kaufman, A., 2000. Timing and hydrological conditions of Sapropel events in the Eastern Mediterranean, as evident from speleothems, Soreq cave, Israel. *Chem. Geol.* 169, 145–156. [https://doi.org/10.1016/S0009-2541\(99\)00232-6](https://doi.org/10.1016/S0009-2541(99)00232-6).
- Barrows, T.T., Williams, M.A.J., Mills, S.C., Duller, G.A.T., Fifield, L.K., Haberlah, D., Tims, S.G., Williams, F.M., 2014. A White Nile megalake during the last interglacial period. *Geology* 42, 163–166. <https://doi.org/10.1130/G35238.1>.
- Bartov, Y., Goldstein, S.L., Stein, M., Enzel, Y., 2003. Catastrophic arid episodes in the eastern Mediterranean linked with the north Atlantic Heinrich events. *Geology* 31 (439). [https://doi.org/10.1130/0091-7613\(2003\)031<0439:CAEITE>2.0.CO;2](https://doi.org/10.1130/0091-7613(2003)031<0439:CAEITE>2.0.CO;2).
- Bastian, L., Revel, M., Bayon, G., Dufour, A., Vigier, N., 2017. Abrupt response of chemical weathering to Late Quaternary hydroclimate changes in northeast Africa. *Sci. Rep.* 7. <https://doi.org/10.1038/srep44231>.
- Béthoux, J.P., Gentili, B., Raunet, J., Tailliez, D., 1990. Warming trend in the western Mediterranean deep water. *Nature* 347, 660–662.
- Bianchi, D., Zavatarelli, M., Pinardi, N., Capozzi, R., Capotondi, L., Corselli, C., Masina, S., 2006. Simulations of ecosystem response during the sapropel S1 deposition event. *Palaeogeogr. Palaeoclimatol. Palaeoecol.* 235, 265–287.
- Blanchet, C.L., Contoux, C., Leduc, G., 2015. Runoff and precipitation dynamics in the Blue and White Nile catchments during the mid-Holocene: a data-model comparison. *Quat. Sci. Rev.* 130, 222–230. <https://doi.org/10.1016/j.quascirev.2015.07.014>.
- Blanchet, C.L., Tjallingii, R., Frank, M., Lorenzen, J., Reitz, A., Brown, K., Feseker, T., Brückmann, W., 2013. High- and low-latitude forcing of the Nile River regime during the Holocene inferred from laminated sediments of the Nile deep-sea fan. *Earth Planet Sci. Lett.* 364, 98–110. <https://doi.org/10.1016/j.epsl.2013.01.009>.
- Bryden, H.L., Candela, J., Kinder, T.H., 1994. Exchange through the Strait of Gibraltar. *Prog. Oceanogr.* 33, 201–248. [https://doi.org/10.1016/0079-6611\(94\)90028-0](https://doi.org/10.1016/0079-6611(94)90028-0).
- Cacho, I., Grimalt, J.O., Canals, M., 2002. Response of the Western Mediterranean Sea to rapid climatic variability during the last 50,000 years: a molecular biomarker approach. *J. Mar. Syst.* 33–34, 253–272. [https://doi.org/10.1016/S0924-7963\(02\)00061-1](https://doi.org/10.1016/S0924-7963(02)00061-1).
- Cacho, I., Grimalt, J.O., Sierro, F.J., Shackleton, N., Canals, M., 2000. Evidence for enhanced Mediterranean thermohaline circulation during rapid climatic coolings. *Earth Planet. Sci. Lett.* 183, 417–429. [https://doi.org/10.1016/S0012-821X\(00\)00296-X](https://doi.org/10.1016/S0012-821X(00)00296-X).
- Castañeda, I.S., Schouten, S., Pätzold, J., Lucassen, F., Kasemann, S., Kuhlmann, H., Schefuß, E., 2016. Hydroclimate variability in the Nile river basin during the past 28,000 years. *Earth Planet Sci. Lett.* 438, 47–56. <https://doi.org/10.1016/j.epsl.2015.12.014>.
- Chen, T.-Y., Stumpf, R., Frank, M., Beldowski, J., Staubwasser, M., 2013. Contrasting geochemical cycling of hafnium and neodymium in the central Baltic Sea. *Geochem. Cosmochim. Acta* 123, 166–180. <https://doi.org/10.1016/j.gca.2013.09.011>.
- Copard, K., Colin, C., Douville, E., Freiwald, A., Gudmundsson, G., de Mol, B., Frank, N., 2010. Nd isotopes in deep-sea corals in the North-eastern Atlantic. *Quat. Sci. Rev.* 29, 2499–2508.
- Cornuault, M., Tachikawa, K., Vidal, L., Guihou, A., Siani, G., Deschamps, P., Bassinot, F., Revel, M., 2018. Circulation changes in the eastern Mediterranean sea over the past 23,000 Years inferred from authigenic Nd isotopic ratios. *Paleoceanogr. Palaeoclimatol.* <https://doi.org/10.1002/2017PA003227>.
- Cornuault, M., Vidal, L., Tachikawa, K., Licari, L., Rouaud, G., Sonzogni, C., Revel, M., 2016. Deep water circulation within the eastern Mediterranean Sea over the last 95 kyr: new insights from stable isotopes and benthic foraminiferal assemblages. *Palaeogeogr. Palaeoclimatol. Palaeoecol.* 459, 1–14. <https://doi.org/10.1016/j.palaeo.2016.06.038>.
- Cramp, A., O'Sullivan, G., 1999. Neogene sapropels in the Mediterranean: a review. *Mar. Geol.* 153, 11–28. [https://doi.org/10.1016/S0025-3227\(98\)00092-9](https://doi.org/10.1016/S0025-3227(98)00092-9).
- De Lange, G.J., Thomson, J., Reitz, A., Slomp, C.P., Principato, M.S., Erba, E., Corselli, C., 2008. Synchronous basin-wide formation and redox-controlled preservation of a Mediterranean sapropel. *Nat. Geosci.* 1, 606–610.
- DeMenocal, P., Ortiz, J., Guilderson, T., Sarnthein, M., 2000. Coherent high- and low-latitude climate variability during the Holocene warm period. *Science* (80-.) 288, 2198–2202. <https://doi.org/10.1126/science.288.5474.2198>.
- Dubois-Dauphin, Q., Montagna, P., Siani, G., Douville, E., Wienberg, C., Hebbeln, D., Liu, Z., Kallel, N., Dapoigny, A., Revel, M., Pons-Branchu, E., Taviani, M., Colin, C., 2017. Hydrological variations of the intermediate water masses of the western Mediterranean Sea during the past 20 ka inferred from neodymium isotopic composition in foraminifera and cold-water corals. *Clim. Past* 13, 17–37. <https://doi.org/10.5194/cp-13-17-2017>.
- Ehrmann, W., Schmiedl, G., Beuscher, S., Krüger, S., 2017. Intensity of African humid periods estimated from Saharan dust fluxes. *PLoS One* 12, e0170989. <https://doi.org/10.1371/journal.pone.0170989>.
- Ehrmann, W., Schmiedl, G., Seidel, M., Krüger, S., Schulz, H., 2016. A distal 140 kyr sediment record of Nile discharge and East African monsoon variability. *Clim. Past* 12, 713–727. <https://doi.org/10.5194/cp-12-713-2016>.
- Ehrmann, W., Seidel, M., Schmiedl, G., 2013. Dynamics of Late Quaternary North African humid periods documented in the clay mineral record of central Aegean Sea sediments. *Global Planet. Change* 107, 186–195. <https://doi.org/10.1016/j.gloplacha.2013.05.010>.
- Emeis, K.-C., Schulz, H., Struck, U., Rossignol-Strick, M., Erlenkeuser, H., Howell, M.W., Kroon, D., Mackensen, A., Ishizuka, S., Oba, T., Sakamoto, T., Koizumi, I., 2003. Eastern Mediterranean surface water temperatures and $\delta^{18}O$ composition during deposition of sapropels in the late Quaternary. *Paleoceanography* 18. <https://doi.org/10.1029/2000PA000617> n/a-n/a.
- Filippidi, A., Triantaphyllou, M.V., De Lange, G.J., 2016. Eastern-Mediterranean ventilation variability during sapropel S1 formation, evaluated at two sites influenced by deep-water formation from Adriatic and Aegean Seas. *Quat. Sci. Rev.* 144, 95–106.
- Fontugne, M., Arnold, M., Labeyrie, L., Paterne, M., Calvert, S.E., Duplessy, J.C., 1994. Paleoenvironment, sapropel chronology and Nile river discharge during the last 20,000 years as indicated by deep-sea sediment records in the eastern Mediterranean. *Radiocarbon* 34, 75–88.
- Foucault, A., Stanley, D.J., 1989. Late Quaternary palaeoclimatic oscillations in East Africa recorded by heavy minerals in the Nile delta. *Nature* 339, 44–46. <https://doi.org/10.1038/339044a0>.
- Freydier, R., Michard, A., De Lange, G., Thomson, J., 2001. Nd isotopic compositions of Eastern Mediterranean sediments: tracers of the Nile influence during sapropel S1 formation? *Mar. Geol.* 177, 45–62. [https://doi.org/10.1016/S0025-3227\(01\)00123-2](https://doi.org/10.1016/S0025-3227(01)00123-2).
- Frigola, J., Moreno, A., Cacho, I., Canals, M., Sierro, F.J., Flores, J.A., Grimalt, J.O., 2008. Evidence of abrupt changes in Western Mediterranean Deep Water circulation during the last 50kyr: a high-resolution marine record from the Balearic Sea. *Quat. Int.* 181, 88–104. <https://doi.org/10.1016/j.quaint.2007.06.016>.
- Garzanti, E., Andò, S., Padoan, M., Vezzoli, G., El Kammar, A., 2015. The modern Nile sediment system: processes and products. *Quat. Sci. Rev.* 130, 9–56. <https://doi.org/10.1016/j.quascirev.2015.07.011>.
- Gasse, F., 2000. Hydrological changes in the African tropics since the last glacial maximum. In: *Quaternary Science Reviews*, pp. 189–211. [https://doi.org/10.1016/S0277-3791\(99\)00061-X](https://doi.org/10.1016/S0277-3791(99)00061-X).
- Goswami, V., Singh, S.K., Bhushan, R., 2014. Impact of water mass mixing and dust deposition on Nd concentration and ϵ_{Nd} of the Arabian Sea water column. *Geochem. Cosmochim. Acta* 145, 30–49. <https://doi.org/10.1016/j.gca.2014.09.006>.
- Grant, K.M., Rohling, E.J., Bronk Ramsey, C., Cheng, H., Edwards, R.L., Florindo, F., Heslop, D., Marra, F., Roberts, A.P., Tamsieia, M.E., Williams, F., 2014. Sea-level variability over five glacial cycles. *Nat. Commun.* 5, 5076.
- Grant, K.M., Grimm, R., Mikolajewicz, U., Marino, G., Ziegler, M., Rohling, E.J., 2016. The timing of Mediterranean sapropel deposition relative to insolation, sea-level and African monsoon changes. *Quat. Sci. Rev.* 140, 125–141. <https://doi.org/10.1016/j.quascirev.2016.03.026>.
- Grimm, R., Maier-Reimer, E., Mikolajewicz, U., Schmiedl, G., Müller-Navarra, K., Adloff, F., Grant, K.M., Ziegler, M., Lourens, L.J., Emeis, K.C., 2015. Late glacial initiation of Holocene eastern Mediterranean sapropel formation. *Nat. Commun.* 6, 7099. <https://doi.org/10.1038/ncomms8099>.
- Henry, F., Jeandel, C., Dupré, B., Minster, J.-F., 1994. Particulate and dissolved Nd in the western Mediterranean Sea: sources, fate and budget. *Mar. Chem.* 45, 283–305. [https://doi.org/10.1016/0304-4203\(94\)90075-2](https://doi.org/10.1016/0304-4203(94)90075-2).
- Incarbona, A., Sprovieri, M., Lirer, F., Sprovieri, R., 2011. Surface and deep water conditions in the Sicily channel (central Mediterranean) at the time of sapropel S5 deposition. *Palaeogeogr. Palaeoclimatol. Palaeoecol.* 306, 243–248. <https://doi.org/10.1016/j.palaeo.2011.04.030>.
- Jacobsen, S.B., Wasserburg, G.J., 1980. Sm-Nd isotopic evolution of chondrites. *Earth Planet Sci. Lett.* 50, 139–155. [https://doi.org/10.1016/0012-821X\(80\)90125-9](https://doi.org/10.1016/0012-821X(80)90125-9).
- Jilbert, T., Reichart, G.J., Aeschlimann, B., Gunther, D., Boer, W., de Lange, G.J., 2010. Climatecontrolled multidecadal variability in North African dust transport to the Mediterranean. *Geology* 38, 19–22.
- Jiménez-Espejo, F.J., Pardos-Gené, M., Martínez-Ruiz, F., García-Alix, A., van de Fliedert, T., Toyofuku, T., Bahr, A., Kreissig, K., 2015. Geochemical evidence for intermediate water circulation in the westernmost Mediterranean over the last

- 20kyrBP and its impact on the Mediterranean Outflow. *Global Planet. Change* 135, 38–46. <https://doi.org/10.1016/j.gloplacha.2015.10.001>.
- Kallel, N., Paterne, M., Labeyrie, L., Duplessy, J.-C., Arnold, M., 1997. Temperature and salinity records of the Tyrrhenian Sea during the last 18,000 years. *Palaeogeogr. Palaeoclimatol. Palaeoecol.* 135, 97–108. [https://doi.org/10.1016/S0031-0182\(97\)00021-7](https://doi.org/10.1016/S0031-0182(97)00021-7).
- Kandiano, E.S., Bauch, H.A., Fahl, K., 2014. Last interglacial surface water structure in the western Mediterranean (Balearic) Sea: climatic variability and link between low and high latitudes. *Global Planet. Change* 123, 67–76. <https://doi.org/10.1016/j.gloplacha.2014.10.004>.
- Krom, M., Cliff, R., Eijsink, L., Herut, B., Chester, R., 1999. The characterisation of Saharan dusts and Nile particulate matter in surface sediments from the Levantine basin using Sr isotopes. *Mar. Geol.* 155, 319–330. [https://doi.org/10.1016/S0025-3227\(98\)00130-3](https://doi.org/10.1016/S0025-3227(98)00130-3).
- Krom, M.D., Stanley, J.D., Cliff, R.A., Woodward, J.C., 2002. Nile River sediment fluctuations over the past 7000 yr and their key role in sapropel development. *Geology* 30, 71. [https://doi.org/10.1130/0091-7613\(2002\)030<0071:NRSFOT>2.0.CO;2](https://doi.org/10.1130/0091-7613(2002)030<0071:NRSFOT>2.0.CO;2).
- Lacan, F., Jeandel, C., 2005. Neodymium isotopes as a new tool for quantifying exchange fluxes at the continent–ocean interface. *Earth Planet. Sci. Lett.* 232, 245–257. <https://doi.org/10.1016/j.epsl.2005.01.004>.
- Lamb, H.F., Bates, C.R., Bryant, C.L., Davies, S.J., Huws, D.G., Marshall, M.H., Roberts, H.M., 2018. 150,000-year palaeoclimate record from northern Ethiopia supports early, multiple dispersals of modern humans from Africa. *Sci. Rep.* 8, 1077. <https://doi.org/10.1038/s41598-018-19601-w>.
- Langgut, D., Almogi-Labin, A., Bar-Matthews, M., Weinstein-Evron, M., 2011. Vegetation and climate changes in the South Eastern Mediterranean during the Last Glacial-Interglacial cycle (86 ka): new marine pollen record. *Quat. Sci. Rev.* 30, 3960–3972. <https://doi.org/10.1016/j.quascirev.2011.10.016>.
- Larrasoana, J.C., Roberts, A.P., Rohling, E.J., Winkhofer, M., Wehausen, R., 2003. Three million years of monsoon variability over the northern Sahara. *Clim. Dynam.* 21, 689–698. <https://doi.org/10.1007/s00382-003-0355-z>.
- Lascaratos, A., Williams, R.G., Tragou, E., 1993. A mixed-layer study of the formation of Levantine intermediate water. *J. Geophys. Res.* 98, 14739. <https://doi.org/10.1029/93JC00912>.
- Lourens, L.J., 2004. Revised Tuning of Ocean Drilling Program Site 964 and KC01B (Mediterranean) and Implications for the δ Sup18sup O (teph.pdf).
- Lugmair, G.W., Shimamura, T., Lewis, R.S., Anders, E., 1983. Samarium-146 in the early solar system: evidence from neodymium in the Allende Meteorite. *Science* (80–222), 1015–1018. <https://doi.org/10.1126/science.222.4627.1015>.
- Malanotte-Rizzoli, P., Manca, B.B., D'Alcala, M.R., Theocharis, A., Brenner, S., Budillon, G., Ozsoy, E., 1999. The Eastern Mediterranean in the 80s and in the 90s: the big transition in the intermediate and deep circulations. *Dynam. Atmos. Oceans* 29, 365–395. [https://doi.org/10.1016/S0377-0265\(99\)00011-1](https://doi.org/10.1016/S0377-0265(99)00011-1).
- Martinez-Ruiz, F., Paytan, A., Kastner, M., González-Donoso, J.M., Linares, D., Bernasconi, S.M., Jimenez-Espejo, F.J., 2003. A comparative study of the geochemical and mineralogical characteristics of the S1 sapropel in the western and eastern Mediterranean. *Palaeogeogr. Palaeoclimatol. Palaeoecol.* 190, 23–37. [https://doi.org/10.1016/S0031-0182\(02\)00597-7](https://doi.org/10.1016/S0031-0182(02)00597-7).
- Martrat, B., Grimalt, J.O., Lopez-Martinez, C., Cacho, I., Sierro, F.J., Flores, J.A., Zahn, R., Canals, M., Curtis, J.H., Hodell, D.A., 2004. Abrupt temperature changes in the Western Mediterranean over the past 250,000 years. *Science* 80 (306), 1762–1765. <https://doi.org/10.1126/science.1101706>.
- Melki, T., Kallel, N., Jorissen, F.J., Guichard, F., Dennielou, B., Berné, S., Labeyrie, L., Fontugne, M., 2009. Abrupt climate change, sea surface salinity and paleo-productivity in the western Mediterranean Sea (Gulf of Lion) during the last 28 kyr. *Palaeogeogr. Palaeoclimatol. Palaeoecol.* 279, 96–113. <https://doi.org/10.1016/j.palaeo.2009.05.005>.
- Ménot, G., Pivrot, S., Bouloubassi, I., Davtian, N., Hennekam, R., Bosch, D., Ducassou, E., Bard, E., Migeon, S., Revel, M., 2020. Timing and stepwise transitions of the African Humid Period from geochemical proxies in the Nile deep-sea fan sediments. *Quat. Sci. Rev.* 228.
- Mercone, D., Thomson, J., Croudace, I.W., Siani, G., Paterne, M., Troelstra, S., Croudace, L.W., Siani, G., Paterne, M., Troelstra, S., 2000. Duration of S1, the most recent sapropel in the eastern Mediterranean Sea, as indicated by accelerator mass spectrometry radiocarbon and geochemical evidence. *Paleoceanography* 15, 336–347. <https://doi.org/10.1029/1999PA000397>.
- Mikolajewicz, U., 2011. Climate of the Past Modeling Mediterranean Ocean Climate of the Last Glacial Maximum, vol. 7, pp. 161–180. <https://doi.org/10.5194/cp-7-161-2011>.
- Millot, C., 1999. Circulation in the western Mediterranean sea. *J. Mar. Syst.* 20, 423–442. [https://doi.org/10.1016/S0924-7963\(98\)00078-5](https://doi.org/10.1016/S0924-7963(98)00078-5).
- Millot, C., Candela, J., Fuda, J.-L., Tber, Y., 2006. Large warming and salinification of the Mediterranean outflow due to changes in its composition. *Deep-Sea Res. Part I Oceanogr. Res. Pap.* 53, 656–666. <https://doi.org/10.1016/j.dsr.2005.12.017>.
- Molina-Kescher, M., Frank, M., Hathorne, E.C., 2014. Nd and Sr isotope compositions of different phases of surface sediments in the South Pacific: extraction of seawater signatures, boundary exchange, and detrital/dust provenance. *Geochemistry, Geophys. Geosystems* 15, 3502–3520. <https://doi.org/10.1002/2014GC005443>.
- Murat, A., Got, H., 2000. Organic carbon variations of the eastern Mediterranean Holocene sapropel: a key for understanding formation processes. *Palaeogeogr. Palaeoclimatol. Palaeoecol.* 158, 241–257.
- Myers, P.G., Haines, K., Rohling, E.J., 1998a. Modeling the paleocirculation of the Mediterranean: the last glacial maximum and the Holocene with emphasis on the formation of sapropel S1. *Paleoceanography* 13, 586–606. <https://doi.org/10.1029/98PA02736>.
- Myers, P.G., Haines, K., Rohling, E.J., 1998b. Myers, Haines, Rohling - 1998 - Modeling the Paleocirculation of the Mediterranean the Last Glacial Maximum and the Holocene with Emphas.Pdf.
- Myers, P.G., 2002. Flux-forced simulations of the paleocirculation of the Mediterranean. *Paleoceanography* 17, 1009. <https://doi.org/10.1029/2000PA000613>.
- Osborne, A.H., Haley, B.A., Hathorne, E.C., Flögel, S., Frank, M., 2014. Neodymium isotopes and concentrations in Caribbean seawater: tracing water mass mixing and continental input in a semi-enclosed ocean basin. *Earth Planet. Sci. Lett.* 406, 174–186. <https://doi.org/10.1016/j.epsl.2014.09.011>.
- Osborne, A.H., Marino, G., Vance, D., Rohling, E.J., 2010. Eastern Mediterranean surface water Nd during Eemian sapropel S5: monitoring northerly (mid-latitude) versus southerly (sub-tropical) freshwater contributions. *Quat. Sci. Rev.* 29, 2473–2483.
- Osborne, A.H., Vance, D., Rohling, E.J., Barton, N., Rogerson, M., Fello, N., 2008. A humid corridor across the Sahara for the migration of early modern humans out of Africa 120,000 years ago. *Proc. Natl. Acad. Sci. United States Am.* 105, 16444–16447.
- Padoan, M., Garzanti, E., Harlavan, Y., Villa, I.M., 2011. Tracing Nile sediment sources by Sr and Nd isotope signatures (Uganda, Ethiopia, Sudan). *Geochim. Cosmochim. Acta* 75, 3627–3644. <https://doi.org/10.1016/j.gca.2011.03.042>.
- Paillard, D., Labeyrie, L., Yiou, P., 1996. Analyseries 1.0: a Macintosh software for the analysis of geographical timeseries. *Eos Trans. AGU* 77, 379.
- Pinardi, N., Masetti, E., 2000. Variability of the large scale general circulation of the Mediterranean Sea from observations and modelling: a review. *Palaeogeogr. Palaeoclimatol. Palaeoecol.* 158, 153–174.
- Piotrowski, A.M., Galy, A., Nicholl, J.A.L., Roberts, N., Wilson, D.J., Clegg, J.A., Yu, J., 2012. Reconstructing deglacial North and South Atlantic deep water sourcing using foraminiferal Nd isotopes. *Earth Planet. Sci. Lett.* 357–358, 289–297. <https://doi.org/10.1016/j.epsl.2012.09.036>.
- Revel, M., Colin, C., Bernasconi, S., Combourieu-Nebout, N., Ducassou, E., Grousset, F.E., Rolland, Y., Migeon, S., Bosch, D., Brunet, P., Zhao, Y., Mascle, J., 2014. 21,000 Years of Ethiopian African monsoon variability recorded in sediments of the western Nile deep-sea fan. *Reg. Environ. Change* 14, 1685–1696. <https://doi.org/10.1007/s10113-014-0588-x>.
- Revel, M., Ducassou, E., Grousset, F.E., Bernasconi, S.M.M., Migeon, S., Revillon, S., Mascle, J., Murat, A., Zaragosi, S., Bosch, D., 2010. 100,000 Years of African monsoon variability recorded in sediments of the Nile margin. *Quat. Sci. Rev.* 29, 1342–1362. <https://doi.org/10.1016/j.quascirev.2010.02.006>.
- Revel, M., Ducassou, E., Skonieczny, C., Colin, C., Bastian, L., Bosch, D., Migeon, S., Mascle, J., 2015. 20,000 years of Nile River dynamics and environmental changes in the Nile catchment area as inferred from Nile upper continental slope sediments. *Quat. Sci. Rev.* 130, 200–221. <https://doi.org/10.1016/j.quascirev.2015.10.030>.
- Roberts, N.L., Piotrowski, A.M., Elderfield, H., Eglinton, T.I., Lomas, M.W., 2012. Rare earth element association with foraminifera. *Geochim. Cosmochim. Acta* 94, 57–71. <https://doi.org/10.1016/j.gca.2012.07.009>.
- Robinson, A.R., Leslie, W.G., Theocharis, A., Lascaratos, A., 2001. Mediterranean sea circulation. *Ocean Curr.* 1, 19.
- Roether, W., Manca, B.B., Klein, B., Bregant, D., Georgopoulos, D., Beitzel, V., Kovacevic, V., Luchetta, A., 1996. Recent changes in eastern Mediterranean deep waters. *Science* 271, 333–335.
- Rohling, E.J., 1994. Review and new aspects concerning the formation of eastern Mediterranean sapropels. *Mar. Geol.* 122, 1–28. [https://doi.org/10.1016/0025-3227\(94\)90202-X](https://doi.org/10.1016/0025-3227(94)90202-X).
- Rohling, E.J., Cane, T.R., Bouloubassi, I., Kemp, A.E.S., Kroon, D., Schiebel, R., Lorre, A., Emeis, K.C., Cooke, S., Jorissen, F.J., Sprovieri, M., 2002. African monsoon variability during the previous interglacial maximum. *Earth Planet. Sci. Lett.* [https://doi.org/10.1016/S0012-821X\(02\)00775-6](https://doi.org/10.1016/S0012-821X(02)00775-6).
- Rohling, E.J., Den Dulk, M., Pujol, C., Vergnaud-Grazzini, C., 1995. Abrupt hydrographic change in the Alboran Sea (western Mediterranean) around 8000 yrs BP. *Deep-Sea Res. Part I Oceanogr. Res. Pap.* 42, 1609–1619. [https://doi.org/10.1016/0967-0637\(95\)00069-1](https://doi.org/10.1016/0967-0637(95)00069-1).
- Rohling, E.J., Marino, G., Grant, K.M., 2015. Mediterranean climate and oceanography, and the periodic development of anoxic events (sapropels). *Earth Sci. Rev.* 143, 62–97. <https://doi.org/10.1016/j.earscirev.2015.01.008>.
- Rosignol-Strick, M., Nesteroff, W., Olive, P., Vergnaud-Grazzini, C., 1982. After the deluge: Mediterranean stagnation and sapropel formation. *Nature* 285, 105–110. <https://doi.org/10.1038/295105a0>.
- Rousseau, T.C.C., Sonke, J.E., Chmieleff, J., van Beek, P., Souhaut, M., Boaventura, G., Seyler, P., Jeandel, C., 2015. Rapid neodymium release to marine waters from lithogenic sediments in the Amazon estuary. *Nat. Commun.* 6, 7592. <https://doi.org/10.1038/ncomms8592>.
- Scheuvs, D., Schütz, L., Kandler, K., Ebert, M., Weinbruch, S., 2013. Bulk composition of northern African dust and its source sediments — a compilation. *Earth Sci. Rev.* 116, 170–194. <https://doi.org/10.1016/j.earscirev.2012.08.005>.
- Schmiedl, G., Kuhnt, T., Ehrmann, W., Emeis, K.-C., Hamann, Y., Kotthoff, U., Dulski, P., Pross, J., 2010. Climatic forcing of eastern Mediterranean deep-water formation and benthic ecosystems during the past 22 000 years. *Quat. Sci. Rev.* 29, 3006–3020. <https://doi.org/10.1016/j.quascirev.2010.07.002>.
- Schmiedl, G., Mitschele, A., Beck, S., Emeis, K.-C., Hemleben, C., Schulz, H., Sperling, M., Weldeab, S., 2003. Benthic foraminiferal record of ecosystem variability in the eastern Mediterranean Sea during times of sapropel S5 and S6

- deposition. *Palaeogeogr. Palaeoclimatol. Palaeoecol.* 190, 139–164. [https://doi.org/10.1016/S0031-0182\(02\)00603-X](https://doi.org/10.1016/S0031-0182(02)00603-X).
- Schroeder, K., García-Lafuente, J., Josey, S.A., Artale, V., Nardelli, B.B., Carrillo, A., Gacic, M., Gasparini, G., Pietro, Herrmann, M., Lionello, P., others, 2012. In: Lionello, P. (Ed.), *Circulation of the Mediterranean Sea and its Variability*. *Clim. Mediterr. Reg.*. Elsevier, pp. 187–256.
- Scrivner, A.E., Vance, D., Rohling, E.J., 2004. New neodymium isotope data quantify Nile involvement in Mediterranean anoxic episodes. *Geology* 32, 565. <https://doi.org/10.1130/G20419.1>.
- Shanahan, T.M., McKay, N.P., Hughen, K.A., Overpeck, J.T., Otto-Bliesner, B., Heil, C.W., King, J., Scholz, C.A., Peck, J., 2015. The time-transgressive termination of the African humid period. *Nat. Geosci.* 8, 140–144. <https://doi.org/10.1038/ngeo2329>.
- Siddall, M., Khatiwala, S., van de Flierdt, T., Jones, K., Goldstein, S.L., Hemming, S.R., Anderson, R.F., 2008. Towards explaining the Nd paradox using reversible scavenging in an ocean general circulation model. *Earth Planet Sci. Lett.* 274, 448–461. <https://doi.org/10.1016/j.epsl.2008.07.044>.
- Sierro, F.J., Hodell, D.A., Curtis, J.H., Flores, J.A., Reguera, I., Colmenero-Hidalgo, E., Bárcena, M.A., Grimalt, J.O., Cacho, I., Frigola, J., Canals, M., 2005. Impact of iceberg melting on Mediterranean thermohaline circulation during Heinrich events. *Paleoceanography* 20. <https://doi.org/10.1029/2004PA001051> n/a-n/a.
- Singh, S.P., Singh, S.K., Goswami, V., Bhushan, R., Rai, V.K., 2012. Spatial distribution of dissolved neodymium and ϵ_{Nd} in the Bay of Bengal: role of particulate matter and mixing of water masses. *Geochem. Cosmochim. Acta* 94, 38–56. <https://doi.org/10.1016/j.gca.2012.07.017>.
- Skonieczny, C., McGee, D., Winckler, G., Bory, A., Bradtmiller, L.L., Kinsley, C.W., Polissar, P.J., De Pol-Holz, R., Rossignol, L., Malaizé, B., 2019. Monsoon-driven Saharan dust variability over the past 240,000 years. *Sci. Adv.* 5 <https://doi.org/10.1126/sciadv.aav1887>.
- Skonieczny, C., Paillou, P., Bory, A., Bayon, G., Biscara, L., Crosta, X., Eynaud, F., Malaizé, B., Revel, M., Aleman, N., Barusseau, J.P., Vernet, R., Lopez, S., Grousset, F., 2015. African humid periods triggered the reactivation of a large river system in Western Sahara. *Nat. Commun.* 6 <https://doi.org/10.1038/ncomms9751>.
- Spivack, A.J., Wasserburg, G.J., 1988. Neodymium isotopic composition of the Mediterranean outflow and the eastern North Atlantic. *Geochem. Cosmochim. Acta* 52, 2767–2773. [https://doi.org/10.1016/0016-7037\(88\)90144-5](https://doi.org/10.1016/0016-7037(88)90144-5).
- Sprovieri, M., Di Stefano, E., Incarbona, A., Salvaggio Manta, D., Pelosi, N., Ribera d'Alcalà, M., Sprovieri, R., 2012. Centennial-scale climate oscillations in the Central-Eastern Mediterranean Sea between 20,000 and 70,000 years ago: evidence from a high-resolution geochemical and micropaleontological record. *Quat. Sci. Rev.* 46, 126–135. <https://doi.org/10.1016/j.quascirev.2012.05.005>.
- Stratford, K., Williams, R.G., Myers, P.G., 2000. Impact of the circulation on sapropel formation in the eastern Mediterranean. *Global Biogeochem. Cycles* 14, 683–695.
- Tachikawa, K., Athias, V., Jeandel, C., 2003. Neodymium budget in the modern ocean and paleo-oceanographic implications. *J. Geophys. Res.* 108, 3254. <https://doi.org/10.1029/1999JC000285>.
- Tachikawa, K., Piotrowski, A.M., Bayon, G., 2014. Neodymium associated with foraminiferal carbonate as a recorder of seawater isotopic signatures. *Quat. Sci. Rev.* 88, 1–13. <https://doi.org/10.1016/j.quascirev.2013.12.027>.
- Tachikawa, K., Roy-Barman, M., Michard, A., Thouron, D., Yeghicheyan, D., Jeandel, C., 2004. Neodymium isotopes in the Mediterranean Sea: comparison between seawater and sediment signals. *Geochem. Cosmochim. Acta* 68, 3095–3106. <https://doi.org/10.1016/j.gca.2004.01.024>.
- Tachikawa, K., Toyofuku, T., Basile-Doelsch, I., Delhaye, T., 2013. Microscale neodymium distribution in sedimentary planktonic foraminiferal tests and associated mineral phases. *Geochem. Cosmochim. Acta* 100, 11–23. <https://doi.org/10.1016/j.gca.2012.10.010>.
- Tachikawa, K., Vidal, L., Cornuault, M., Garcia, M., Pothin, A., Sonzogni, C., Bard, E., Menot, G., Revel, M., 2015. Eastern Mediterranean Sea circulation inferred from the conditions of S1 sapropel deposition. *Clim. Past* 11, 855–867. <https://doi.org/10.5194/cp-11-855-2015>.
- Tesi, T., Asioli, A., Minisini, D., Maselli, V., Valle, G.D., Gamberi, F., Langone, L., Cattaneo, A., Montagna, P., Trincardi, F., 2017. Large-scale response of the Eastern Mediterranean thermohaline circulation to African monsoon intensification during sapropel S1 formation. *Quat. Sci. Rev.* 159, 139–154.
- Thunell, R.C., Williams, D.F., 1989. Glacial–Holocene salinity changes in the Mediterranean Sea: hydrographic and depositional effects. *Nature* 338, 493–496. <https://doi.org/10.1038/338493a0>.
- Toucanne, S., Jouet, G., Ducassou, E., Bassetti, M.A., Dennielou, B., Angue Minto'o, C.M., Lahmi, M., Touyet, N., Charlier, K., Lericolais, G., Mulder, T., 2012. A 130,000-year record of levantine intermediate water flow variability in the corsica trough, western Mediterranean sea. *Quat. Sci. Rev.* 33, 55–73. <https://doi.org/10.1016/j.quascirev.2011.11.020>.
- Toucanne, S., Minto'o, C.M.A., Fontanier, C., Bassetti, M.A., Jorry, S.J., Jouet, G., 2015. Tracking rainfall in the northern Mediterranean borderlands during sapropel deposition. *Quat. Sci. Rev.* 129, 178–195.
- Vadsaria, T., Ramstein, G., Dutay, J.-C., Li, L., Ayache, M., Richon, C., 2019. Simulating the occurrence of the last sapropel event (S1): Mediterranean basin ocean dynamics simulations using Nd isotopic composition modeling. *Paleoceanogr. Paleoclimatol.* 34, 237–251. <https://doi.org/10.1029/2019PA003566>.
- Vance, D., Burton, K.W., 1999. Neodymium isotopes in planktonic foraminifera: a record of the response of continental weathering and ocean circulation rates to climate change. *Earth Planet Sci. Lett.* 173, 365–379. [https://doi.org/10.1016/S0012-821X\(99\)00244-7](https://doi.org/10.1016/S0012-821X(99)00244-7).
- Vance, D., Scrivner, A.E., Beney, P., 2004. The use of foraminifera as a record of the past neodymium isotope composition of seawater. *Paleoceanography* 19. <https://doi.org/10.1029/2003PA000957>. PA2009–PA2009.
- Wehausen, R., Brumsack, H.-J., 1999. Cyclic variations in the chemical composition of eastern Mediterranean Pliocene sediments: a key for understanding sapropel formation. *Mar. Geol.* 153, 161–176. [https://doi.org/10.1016/S0025-3227\(98\)00083-8](https://doi.org/10.1016/S0025-3227(98)00083-8).
- Weldeab, S., Emeis, K.-C., Hemleben, C., Siebel, W., 2002a. Provenance of lithogenic surface sediments and pathways of riverine suspended matter in the Eastern Mediterranean Sea: evidence from $^{143}\text{Nd}/^{144}\text{Nd}$ and $^{87}\text{Sr}/^{86}\text{Sr}$ ratios. *Chem. Geol.* 186, 139–149. [https://doi.org/10.1016/S0009-2541\(01\)00415-6](https://doi.org/10.1016/S0009-2541(01)00415-6).
- Weldeab, S., Emeis, K.-C., Hemleben, C., Vennemann, T.W., Schulz, H., 2002b. Sr and Nd isotope composition of Late Pleistocene sapropels and nonsapropelic sediments from the Eastern Mediterranean Sea: implications for detrital influx and climatic conditions in the source areas. *Geochem. Cosmochim. Acta* 66, 3585–3598. [https://doi.org/10.1016/S0016-7037\(02\)00954-7](https://doi.org/10.1016/S0016-7037(02)00954-7).
- Williams, M.A., Adamson, D., Cock, B., McEvedy, R., 2000. Late quaternary environments in the white Nile region, Sudan. *Global Planet. Change* 26, 305–316. [https://doi.org/10.1016/S0921-8181\(00\)00047-3](https://doi.org/10.1016/S0921-8181(00)00047-3).
- Wu, J., Böning, P., Pahnke, K., Tachikawa, K., de Lange, G.J., 2016. Unraveling North-African riverine and eolian contributions to central Mediterranean sediments during Holocene sapropel S1 formation. *Quat. Sci. Rev.* 152, 31–48. <https://doi.org/10.1016/j.quascirev.2016.09.029>.
- Wu, J., Liu, Z., Stuu, J.-B., Zhao, Y., Schirone, A., Lange, G.-J., 2017. North-African paleodrainage discharges to the central Mediterranean during the last 18,000 years: a multiproxy characterization. *Quat. Sci. Rev.* 163, 95–113.
- Wu, J., Pahnke, K., Böning, P., Wu, L., Michard, A., de Lange, G.J., 2019. Divergent Mediterranean seawater circulation during Holocene sapropel formation – reconstructed using Nd isotopes in fish debris and foraminifera. *Earth Planet Sci. Lett.* 511, 141–153. <https://doi.org/10.1016/j.epsl.2019.01.036>.
- Wu, Q., Colin, C., Liu, Z., Douville, E., Dubois-Dauphin, Q., Frank, N., 2015a. New insights into hydrological exchange between the South China Sea and the Western Pacific Ocean based on the Nd isotopic composition of seawater. *Deep Sea Res. Part II Top. Stud. Oceanogr.* 122, 25–40. <https://doi.org/10.1016/j.dsr2.2015.11.005>.
- Wu, Q., Colin, C., Liu, Z., Thil, F., Dubois-Dauphin, Q., Frank, N., Tachikawa, K., Bordier, L., Douville, E., 2015b. Neodymium isotopic composition in foraminifera and authigenic phases of the South China Sea sediments: implications for the hydrology of the North Pacific Ocean over the past 25 kyr. *Geochemistry, Geophys. Geosystems* 16, 3883–3904. <https://doi.org/10.1002/2015GC005871>.
- Xu, Z., Li, T., Colin, C., Clift, P.D., Sun, R., Yu, Z., Wan, S., Lim, D., 2018. Seasonal variations in the Siliciclastic fluxes to the western Philippine Sea and their impacts on seawater ϵ_{Nd} values inferred from 1 Year of in Situ observations above Benham rise. *J. Geophys. Res. Ocean.* 123, 6688–6702. <https://doi.org/10.1029/2018JC014274>.
- Yu, Z., Colin, C., Ma, R., Meynadier, L., Wan, S., Wu, Q., Kallel, N., Sepulcre, S., Dapoigny, A., Bassinot, F., 2018. Antarctic intermediate water penetration into the northern Indian ocean during the last deglaciation. *Earth Planet Sci. Lett.* 500, 67–75. <https://doi.org/10.1016/j.epsl.2018.08.006>.
- Zhao, Y., Colin, C., Liu, Z., Paterne, M., Siani, G., Xie, X., 2012. Reconstructing precipitation changes in northeastern Africa during the Quaternary by clay mineralogical and geochemical investigations of Nile deep-sea fan sediments. *Quat. Sci. Rev.* 57, 58–70. <https://doi.org/10.1016/j.quascirev.2012.10.009>.
- Zhao, Y., Liu, Z., Colin, C., Paterne, M., Siani, G., Cheng, X., Duchamp-Alphonse, S., Xie, X., 2011. Variations of the Nile suspended discharges during the last 1.75 Myr. *Palaeogeogr. Palaeoclimatol. Palaeoecol.* 311, 230–241. <https://doi.org/10.1016/j.palaeo.2011.09.001>.